Electrophoresis of Large DNA with a Sparse Zinc Oxide Nanowire Array

A THESIS
SUBMITTED TO THE FACULTY OF THE GRADUATE SCHOOL
OF THE UNIVERSITY OF MINNESOTA
BY

Noritoshi Araki

IN PARTIAL FULFILLMENT OF THE REQUIREMENTS
FOR THE DEGREE OF
MASTER OF SCIENCE

Kevin Dorfman, Eray Aydil

May 2010

Acknowledgements

I would like to take an opportunity to express my gratitude to people who have contributed to my graduate study. I am very thankful to my advisors, Kevin Dorfman and Eray Aydil, for all the supports they gave me. Jia Ou has been my great mentor since the beginning of my research work. I am thankful for his help. I am also grateful for Nabil Laachi, Maggie Linak, and Dan Olson for their help and advices. They have been a great help understanding the materials related to my research. Lastly, I want to express my gratitude to MRSEC and Packard Fellowship for supporting my M.S. study; this research was supported by the MRSEC Program of the National Science Foundation under Award Number DMR-0819885 and the David and Lucile Packard Foundation.

Abstract

We developed a simple inexpensive method to integrate ZnO nanowires into a microchannel using a combination of aqueous solution synthesis of ZnO nanowires and photolithography, which is used as a nanowire-embedded microfluidic device. The density of ZnO nanowires inside the microchannel is controllable by simply changing the concentration of the seed solution. We conducted a study of dynamic interactions between electric field driven λDNA and a single isolated ZnO nanowire using single molecule spectroscopy technique. The study shows that the hooking time is exponentially dependent on b/R_g, in agreement with a prediction by simulation work. We also find that the hooking probability for small values of b/R_g increases as the electric field strength increases.

Table of Contents

List of Figures

List of Symbols

a	pore size
b	offset of molecule center of mass and center of obstacle
D	diffusion coefficient of a polymer chain
De	Deborah number
c	concentration
d_+	diffusion length in positive x-direction
d_-	diffusion length in negative x-direction
E	electric field
e	fundamental charge, 1.602×10^{-19} C
ϵ	permittivity or dimensionless electric field
ϵ_0	permittivity of free space, 8.854×10^{-12} F/m
F	force
F_f	drag force
F_e	electrophoretic force
h_x	end to end distance in x-direction
I	ionic strength
k_B	Boltzmann constant, 1.381×10^{-23} J/K
κ^{-1}	Debye length
L	contour length
$\mathcal{L}$	length of a stretched chain
l_B	Bjeruum length
l_k	Kuhn length
l_p	persistence length
l_1	length of longer arm
l_2	length of shorter arm
η	liquid viscosity
μ	electrophoretic mobility
μ_x	electrophoretic mobility in x-direction in a tube

N	number of polymerization
N_b	number of ideal blobs
N_k	number of Kuhn steps in the polymer
Pe	Peclet number
Q	total chain charge
q_b	charge on a blob
q_k	charge on a Kuhn segment
R	radius of a polymer chain
R_g	radius of gyration of a polymer chain
R_{obs}	obstacle radius
σ	charge density
T	temperature
t	unhooking time
t_d	thickness of large well in entropic trapping
t_H	hold up time for a post collision
t_s	thickness of channel in entropic trapping
τ	relaxation time of a polymer chain
v	velocity
v_{tube}	velocity along the tube
v_x	velocity in x-direction
ν	Flory exponent
ξ_c	friction coefficient of a polymer chain
ξ_k	friction coefficient of a Kuhn segment
ϕ	ratio of stretched chain length to contour length
λ	effective charge per length
z	valence charge

Chapter 1

DNA Electrophoresis: Background

1.1 Introduction

Electrophoresis is the motion of charged particles under the influence of an electrostatic force. In general, DNA electrophoresis refers to separation of DNA fragments by size under the influence of an electric field. DNA electrophoresis is an important analytical technique in many areas of science including molecular biology, genetics, and forensics. A few of the most important applications such as genome mapping and DNA fingerprinting require separation of large DNA fragments. DNA fingerprinting, for example, has been used as a tool for personal identification, paternity testing, and genetic disease analysis [1–3], and the technique is based on the variations of DNA sequences in key portions of DNA. Prior to analyzing the differences in base sequence or the length of a specific repeat unit in a region of DNA, the DNA removed from the sample cell has to be digested at specific sites by restriction enzymes, and these DNA fragments have to be ordered by length.

Agarose or polyacrylamide gel electrophoresis is commercially available and one of the most standard techniques for DNA electrophoresis. Polyacrylamide gels, having smaller pore sizes than agarose gels, are used for separation of DNA molecules smaller than a few hundred base pairs (bp). Larger DNA molecules are separated by agarose gels. While gel electrophoresis works well for small DNA, its efficiency deteriorates drastically for DNA molecules larger than $\approx$ 40,000 bp. To circumvent this problem, large DNA molecules are more commonly separated with pulsed-field gel electrophoresis (PFGE), in which the direction of the electric field is switched periodically. PFGE enables the separation of DNA molecules up to mega base pairs. However, the separation process is slow, taking up to a few days.

Non-gel separation methods have been investigated as an alternative for faster separation of large DNA molecules over the last several years [4–10]. Even though these non-gel separation methods have demonstrated an order of magnitude faster separation of large DNA than PFGE, these devices still remain in the realm of research laboratories due to their costs and often complicated fabrication techniques.

In this thesis, zinc oxide (ZnO) nanowires are proposed and investigated as novel point-size obstacles for DNA electrophoresis. This thesis begins with the background on DNA electrophoresis. The second chapter discusses some of the non-gel separation techniques. The third chapter discusses the fabrication of ZnO nanowires and the assembling of the microfluidic chip we developed. The thesis concludes with the discussion of our study of electrophoretic interaction of large DNA with an isolated single nanowire.

1.2 DNA as a polyelectrolyte

DNA, the abbreviation of deoxyribonucleic acid, is a nucleic acid that contains genetic information. DNA exists in a famous double helical form,

which consists of two twisting polymer chains of monomer nucleotides. Each nucleotide is made of a deoxyribose sugar, a phosphate group, and one of four bases, adenine, cytosine, guanine, or thymine. The backbone of DNA is composed of alternating deoxyribose sugar and phosphate groups. A base pair (bp) refers to the pairing of two nucleotides across the double helix through hydrogen bonding. Typically only cytosine-guanine pairing or adenine-thymine pairing (Watson-Crick base pairing) are possible in DNA.

DNA is a neutral molecule in a dry state. However, when DNA is placed in an ionic solution like water, the phosphate groups in the backbone dissociate, forming a negatively charged macroion and its counterions in solution. Consequently, this leads to the formation of an electrical double layer on the surface of the polyelectrolyte (Figure 1.1). In close proximity to the macroion, the positive charges are strongly attracted to the negatively charged macroion surface. This thin layer, where the counterions are permanently adsorbed onto the macroion surface, is referred to as Stern layer [11, 12], and it has a typical length of ≈ 1 nm. Outside the Stern layer, there is a second layer where the electric force is not strong enough to bind the counterions to the polyelectrolyte surface. In this layer, the electrostatic attractive force is balanced by diffusion, which tries to randomize the counterions. This second layer outside the Stern layer is called Debye layer [11, 12], and the length of the Debye layer is defined as κ^{-1}. The Debye layer of DNA in a typical electrophoresis buffer has a length of 1-10 nm. Debye length is expressed as

$$\kappa^{-1} = \sqrt{\frac{\epsilon_o \epsilon k_B T}{2e^2 I}} \tag{1.1}$$

with

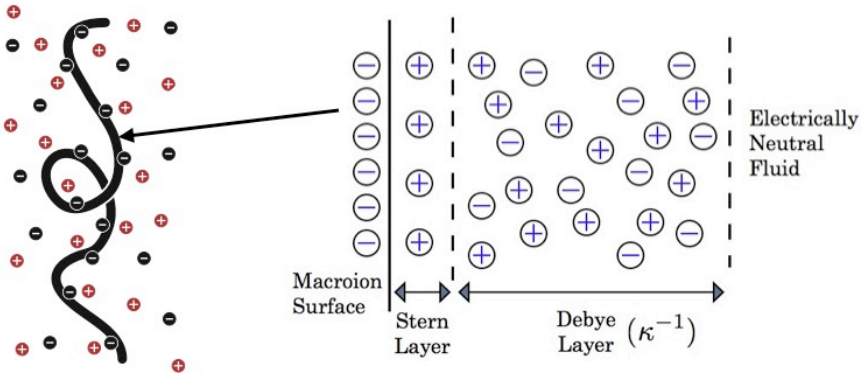

Figure 1.1: *Schematic of electrical double layer. Courtesy of Michel Gauthier.*

$$I = \frac{1}{2}\sum_{i=1}^{n} z_i^2 c_i \tag{1.2}$$

where $\epsilon_o, \epsilon, k_B, T, e, I, z_i$, and c_i, are vacuum permittivity, dielectric constant, Boltzmann constant, temperature, fundamental charge of an electron, ionic strength, valence of ion i, and concentration of ion i, respectively.

When the counterions dissociate, there are two competing effects: i) thermal energy (thermal motion), which tends to randomize the motion of the ions, and ii) electrostatic energy, which tends to bring the ions close to the macroion surface. Bjerrum length, l_B, is a distance at which the thermal energy is balanced by electrostatic energy, and it is given by [12]

$$l_B = \frac{e^2}{4\pi\epsilon_o\epsilon k_B T}. \tag{1.3}$$

Below the Bjerrum length, electrostatic interaction dominates thermal energy, and above the Bjerrum length, it is vice versa.

Manning condensation, proposed in 1969, is a process in which the counterions condense onto the chain until the effective charge spacing is increased and becomes equal to l_B [13]. For example, each base pair of DNA has a

length of 0.34 nm and carries two electron charges, corresponding to charge density $\sigma \approx 6$ e/nm. Bjerrum length in water is 0.7 nm, corresponding to a critical charge density of $\sigma_c \approx 1.4$ e/nm. Manning condensation dictates that the counterions are condensed onto the macroion surface until the effective charge separation becomes equal to Bjerrum length. Because of Manning condensation, the effective charge density of DNA is lower than would be expected in its absence; Manning condensation sets an upper limit for the charge density of DNA.

1.3 Conformation and size of DNA

In polymer physics, the transition from rigid rod to flexible chain is described by the persistence length, l_p, which depends on the surrounding medium of the polymer chain. A polymer chain shorter than the persistence length behaves like a rigid rod, and a chain much larger than the persistence length behaves like a flexible chain. The Kuhn length l_k, which is often used in place of persistence length, is equal to twice the persistence length. For example, DNA in free solution has a Kuhn length of 100 nm, corresponding to ≈ 300 bp (one base pair ≈ 0.34 nm). λ-DNA, which has ≈ 49 kbp, consists of ≈ 160 Kuhn steps, therefore, it is considered a flexible chain. By defining the number of Kuhn segments in the polyelectrolyte as N_k, the contour length of the chain is expressed as $L = N_k l_k$.

A DNA chain is not fully stretched in free solution due to the correspoding entropic penalty. Instead, a DNA molecule forms a random coil. The size of such a coil depends on monomer-monomer interactions, monomer-solvent interactions, and the number of Kuhn segments in the molecule. For an ideal chain (Gaussian) in which segments can occupy the same location simultaneously, the mean square end-to-end distance of a freely jointed chain with N_k Kuhn segments can be given as,

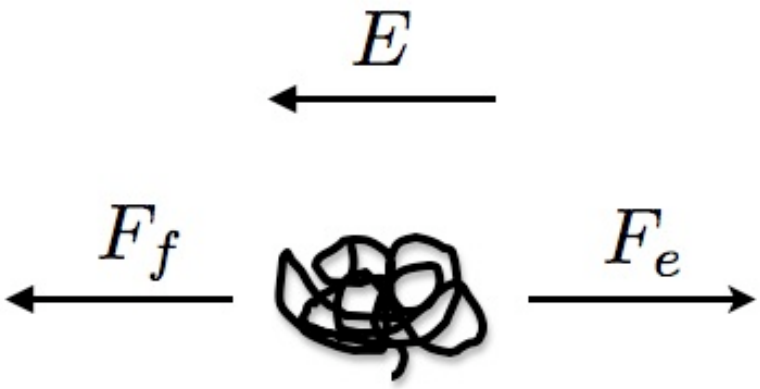

Figure 1.2: *Simple schematic of free solution electrophoresis.*

$$R = N_k^{\frac{1}{2}} l_k. \tag{1.4}$$

Considering the excluded volume effect, the size of the coil is more generally written as

$$R = N_k^{\nu} l_k \tag{1.5}$$

where ν is called Flory exponent and has a value of $\approx 3/5$ for a swelled coil. A radius of gyration, R_g, which is the average distance between the chain segments and the center of mass, is also useful for expressing the polymer size; it has a form [14]

$$R_g = \frac{R}{\sqrt{6}}. \tag{1.6}$$

1.4 Rouse model of DNA hydrodynamics

Next we consider the hydrodynamics of a DNA molecule in an ionic solution subject to an externally applied electric field E (see Figure 1.2). Because of the negatively charged phosphate groups in its backbone, DNA moves in response to an electric field following the Rouse model of hydrodynamics. In the Rouse model, the molecule is freely draining so that each Kuhn segment acts as an independent friction center with a friction coefficient ξ_k and a charge q_k. Therefore, the total friction coefficient and total charge on the random coil are $N_k\xi_k$ and N_kq_k, respectively. The electric force acting on the coil is $F_e = QE = N_kq_kE$, and the total drag force on the coil is $F_f = \xi v = N_k\xi_k v$ with v as the velocity of the molecule. Balancing the electric force and the drag force, the velocity of the polyelectrolyte is

$$v = \frac{N_kq_kE}{N_k\xi_k} = \frac{q_k}{\xi_k}E \tag{1.7}$$

and the free solution electrophoretic mobility is given by

$$\mu = \frac{v}{E} = \frac{q_k}{\xi_k}. \tag{1.8}$$

This expression shows that the free solution mobility of a polyelectrolyte is independent of molecular weight, and thus we are unable to separate molecules by size through simple free solution electrophoresis (there are some exceptions for very short DNA [15]). This fact is the main motivation for the development of various DNA electrophoresis techniques.

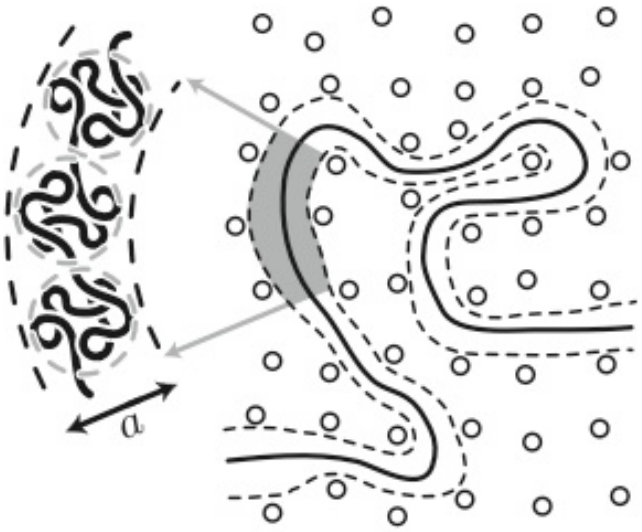

Figure 1.3: *Simple schematic of the reptation model. Courtesy of Michel Gauthier.*

1.5 Reptation: Theory behind gel electrophoresis

The previous section showed that DNA molecules cannot be size-separated by simple free solution electrophoresis. Length-separation requires some additional mechanism to lend a size-dependent mobility. Gel electrophoresis is one of the most widely used techniques for the separation of DNA fragments by size. In gel electrophoresis, porous gel acts as a sieving matrix for DNA molecules. Large DNA molecules have more difficulty moving through the gel pores than smaller DNA because of their size. A simple model to describe the dynamics of DNA molecules through the gel pores is the Biased Reptation model. This model, owing largely to pioneering work of Lerman and Frisch [16] and Lumpkin and Zimm [17], describes the motion of the polymer chain through the randomly distributed obstacles (tube) with a snake-like motion called reptation (Figure 1.3). The DNA molecule is modeled as a

chain comprised of N_b blobs. The size of each blob, a, is the same as the size of the pores. It is assumed that the chain is flexible on a scale of a blob so that inside blob, the chain is still Gaussian ($\nu \approx 1/2$). The total number of blobs in a tube is equal to the total number of Kuhn segments divided by the number of Kuhn segments in one blob, thus

$$N_b = \frac{N_k l_k^2}{a^2}. \tag{1.9}$$

When the chain moves through the tube due to diffusion in the absence of an electric field, each blob experiences a friction force, and the friction force acting on a blob is independent of the other blobs. Therefore, the total friction acting on the chain is

$$\xi_c = N_b \xi_b. \tag{1.10}$$

Using this expression, the diffusion coefficient of the chain is given as

$$D = \frac{k_B T}{\xi_c} = \frac{k_B T}{\xi_b N_b}. \tag{1.11}$$

Next, consider a case in which an external electric field is applied to DNA reptating in a gel. If the field is applied in the x-direction, each blob experiences a force depending on its orientation relative to the applied field. The sum of the electric forces acting on the chain is the sum of the forces acting on each blob. It is given by

$$F = \sum_{i=1}^{N_b} (q_b E) s_i = \frac{QEa}{L} \sum_{i=1}^{N_b} s_i = \frac{QE}{L} h_x \tag{1.12}$$

with $Q = N_b q_b$ total charge of the chain, $L = N_b a$ contour length of the chain, s_i orientation of i-th blob in the x-direction, and h_x end-to-end distance of the

chain in x-direction. Balancing the electric force and friction force gives

$$\xi_c v_{tube} = \frac{QE}{L} h_x \tag{1.13}$$

where v_{tube} is the velocity of the chain along the tube. The translational velocity in the x-direction is related to the curvilinear velocity by [17]

$$v_x = v_{tube} \frac{h_x}{L}. \tag{1.14}$$

Substituting Eq (1.14) into Eq (1.13) and averaging over all tube conformation, the velocity in the x-direction is

$$v_x = \frac{QE}{\xi_c} \left\langle \frac{h_x^2}{L^2} \right\rangle. \tag{1.15}$$

Electrophoretic mobility of the chain in a gel is then given as

$$\mu_x = \frac{v_x}{E} = \frac{Q}{\xi_c} \left\langle \frac{h_x^2}{L^2} \right\rangle = \mu \frac{\langle h_x^2 \rangle}{L^2}. \tag{1.16}$$

If the applied field is weak such that $q_k Ea/k_B T \ll 1$, the chain is not greatly stretched and follows Gaussian statistics so that $\langle h_x \rangle^2 \approx L$. Thus, it shows the size-dependence of mobility, $\mu_x \approx 1/\mathrm{L}$. This case is called biased-reptation without orientation since the chain does not have directional orientation. If the field is strong (though still satisfying $q_k Ea/k_B T < 1$ to prevent tube leakage), the chain will be almost fully stretched so that $\langle h_x \rangle \approx L$ and $\mu_x \approx \mu$. This is called biased-reptation with orientation and it does not show a size-dependent mobility.

1.6 Pulsed-field gel electrophoresis

The experimental results [18] and further derivation of the Biased Reptation Model with fluctuations [19] show that the electrophoretic mobility scales like

$$\frac{\mu_x}{\mu} \approx \frac{\alpha}{N_k} + \beta\epsilon \tag{1.17}$$

where α and β are constants and $\epsilon = q_k Ea/k_B T$, a dimensionless electric field. The transition from unoriented regime to oriented regime occurs when $1/N_k \approx \epsilon$. This shows that for large DNA, it is necessary to use an even smaller field strength to prevent the onset of the oriented regime. The electrophoretic mobility decreases as the allowed field strength is reduced, and it becomes difficult to observe an appreciable migration of DNA through gel. As the field strength is increased, the chain becomes oriented along the field, and the mobility becomes independent of the size. Therefore, large DNA is unable to be separated with a DC field. To circumvent this problem, pulsed-field gel electrophoresis was introduced [20], in which the direction of the electric field is switched periodically. As explained in the previous section, the mobility becomes independent of size once the molecule is oriented with the field. The idea of a pulsed-field is to reorient the molecule by changing the direction of electric field. The time required to reorient along the direction of the new electric field depends on the size of the molecule. Smaller molecules reorient themselves faster in response to the field and can move faster through the gel. Even though the pulsed-field gel electrophoresis realizes the separation of large molecules, the separation process is slow, requiring hours to days to complete the separation [21, 22].

1.7 Capillary electrophoresis

Capillary electrophoresis (CE) is a more recently developed technique and has gained its reputation due to its improved resolution and separation time. This technique uses a narrow capillary tube, typically fused silica with an internal diameter of 50-100 μm and a length of 10-50 cm [12] for separation. The capillary tube is filled with polymer solution (sieving matrix), and the separation occurs as DNA molecules migrate through the sieving matrix inside the tube. One of the advantages of CE is that it allows the use of a higher electric field (typically 200-300 V/cm compared to 50 V/cm in conventional gel electrophoresis); because of the high surface area to volume ratio in a capillary, Joule heat is more efficiently dissipated than in a gel slab, enabling use of higher electric fields. Sample injection is generally performed automatically, and the detection is done by UV absorption or laser-induced fluorescence [12]. CE is the current industrial standard for analytical separation of short DNA. However, it has problems separating large DNA ($>$ 40 kbp) for the same reason as gel electrophoresis. Separation of large DNA (up to mega bp) within an hour has been reported using pulsed-field capillary electrophoresis [22, 23].

Chapter 2

Non-Gel DNA Electrophoresis

The current research trend in DNA electrophoresis is the integration of a separation system on a single chip, which enables faster and more efficient separation of large DNA. Various separation techniques have been proposed and investigated using materials such as silicon, glass, and plastic. Silicon-based materials are a frequent choice because of their compatibility with micro- and nano- electronic fabrication techniques. This chapter discusses some of the new separation techniques and is concluded with an introduction of zinc oxide (ZnO) nanowires as potential separation media.

2.1 Pulsed field in micropost array

Bakajin *et al.* [4] showed the separation of large DNA in microfabricated hexagonal arrays under a pulsed-field. They fabricated a hexagonal array of 2 μm pillars with 2 μm spacings between the pillars on a silica substrate by photolithography and reactive ion etching (RIE) and sealed the chip with a glass cover slip coated with a silicone elastomer. Applying a pulsed electric field along the alternating axes of the array, separated by 120° (see Figure

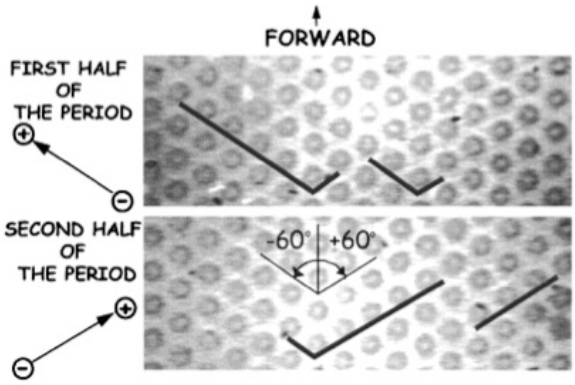

Figure 2.1: *Pulsed field electrophoresis in hexagonal post array. Reprinted from [4].*

2.1), they demonstrated a separation of T4 ($\approx$ 169 kbp) and λ-DNA ($\approx$ 49 kbp) in 10 seconds.

The separation depends on the size-dependent average velocity of the molecules. Shorter molecules move faster in the array because once they reorient themselves along the axis of the field, they can move in a straight direction without hindrance while longer chains have to spend more time retracting their paths under pulsed field as shown in Figure 2.1. Using the assumption that a molecule is uniformly stretched during this motion, the net velocity, v, of a molecule of length L in the pulsed field array is described by [24]

$$v = \mu E \cos\left(\frac{\theta}{2}\right)\left[1 - \frac{L}{L^*}\right] \tag{2.1}$$

where θ is the angle between the transverse fields (in this case 120°), μ is the continuous field mobility, and L^* is a critical cutoff length which arises from the fact that the molecules which do not have time to reorient completely during a single pulse retrace the same path repeatedly, hence making their net velocity zero. By appropriate adjustment of field strength, pulse time,

and array parameters such as the pillar size and spacing, this method can be applied to various sizes of DNA molecules.

2.2 Entropic trapping

Han *et al.* [25] showed a separation of long DNA (5-160 kbp) in a microfabricated entropic array within 15 minutes. The basic design of the entropic array consists of alternating thin and thick regions in a microchannel (see Figure 2.2) fabricated by photolithography and etching techniques on a silicon substrate, which is anodically bonded (sealed) with a glass coverslip. The channel depth of the thin region is smaller than the radius of gyration R_g of the DNA molecules, and the thick region has a depth that is larger than R_g. When driven by the applied electric field, DNA molecules move through the alternating thick and thin regions by changing their conformations repeatedly. When a DNA is in the thick region, its conformation is an equilibrium random coil. As DNA molecules reach the entrance of the thin region, they are trapped temporarily due to the required conformation change to enter the thin region. This conformation change costs entropic energy. To escape from the trap, a sufficient number of DNA monomers have to enter into the thin region. When a sufficient number of DNA monomers are introduced into the thin region by a combination of Brownian motion and electrophoretic force, the escape of the whole molecule from the trap begins [26]. Escape time probability depends upon the surface area of molecule that is in contact with the boundary. Large molecules have a larger surface area in contact with the boundary than the smaller molecules. Therefore, large molecules have higher probability of escaping per unit time, which leads to shorter trapping time and thus higher mobility than the small molecules. Therefore, large molecules migrate through the channel faster than small molecules. Effective separation is observed after the molecules passed a large

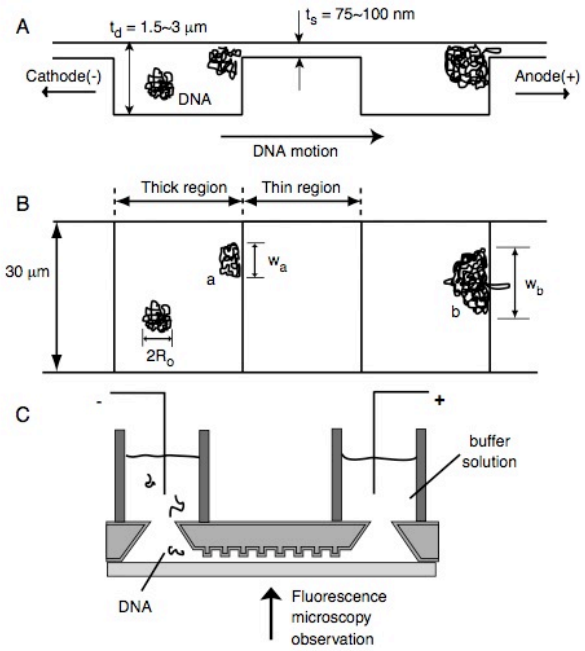

Figure 2.2: *Experimental setup for entropic trapping. Reprinted from [25].*

number of entropic arrays.

2.3 Separation by entropic recoiling

When a DNA coil is forced into a confined space, the free energy of the molecule increases because its entropy is reduced due to a reduced number of possible chain conformations. If there exists an abrupt interface between regions that produce high entropy (unconfined region) and low entropy (confined area), and the molecule is only partially confined to the low entropy region, the entropic force drives the molecule out of the confined region in order to maximize its entropy [27]. If the chain is completely contained in the low entropy region or completely in the high entropy region, the molecule does not experience such a force.

Cabodi *et al.* [28] used this concept for the separation of DNA of dissimilar lengths. Cabodi *et al.* fabricated a dense array of nano-pillars (pillar diameter ≈ 80 nm and pillar spacing ≈ 140 nm), an entropically unfavorable region, in the microchannel by electron beam lithography technologies (for details of the fabrication, refer to [28]). Their separation mechanism is as follows. The DNA molecules are first accumulated at the interface of the dense nanopillar array by a subcritical electric field, which is below the field strength required for insertion of molecules into the pillar region. Next, a high field pulse, which is well above the critical field strength, is applied to the channel. As the high field pulse begins, the molecules reptate into the dense pillar array. At the end of the pulse, some of the molecules have completely entered the dense array while others (larger molecules) are only partially in the pillar array. When the field is turned off, the molecules that are only partially in the dense array retract themselves into the free region due to the entropic force, while the molecules that are completely in the dense array will remain stationary; thus, it leads to a separation by size. By repeating this process and by changing the duration of the pulse-field, it was demonstrated that the separation of mixture of DNA molecules by size can be accomplished. Figure 2.3 illustrates the overall process of the separation.

2.4 Separation by diffusion: Brownian ratchet

According to the Zimm model of diffusion, the friction coefficient of a polymer coil is proportional to the coil size, R_g, and the diffusion coefficient of the coil is approximated as [29]

$$D = \frac{k_B T}{\xi_c} \sim \frac{k_B T}{\eta R_g} \tag{2.2}$$

where ξ and η are the friction coefficient of the chain and the viscosity of

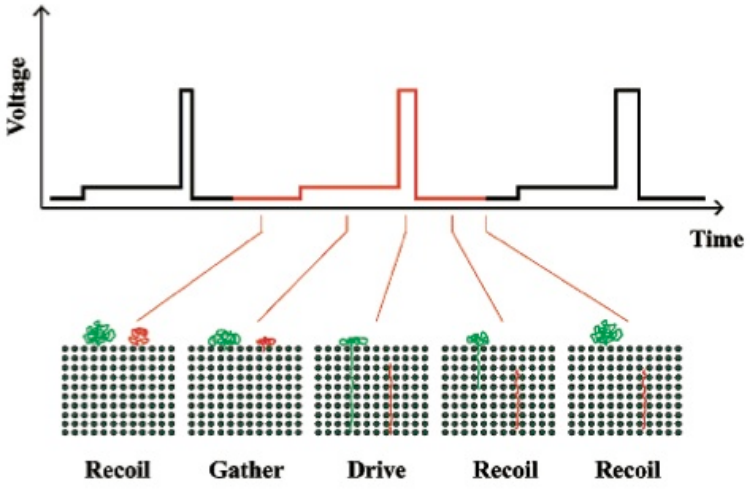

Figure 2.3: *Schematic of separating molecules by entropic recoil. Reprinted from [28].*

the medium, respectively. The equation shows that the shorter chains diffuse faster than the longer chains. Duke and Austin [29] and Ertas [30] proposed a method to separate DNA fragments according to size with this concept. Their proposed design consists of a periodic array of rectangular obstacles which are tilted at a 45° angle with respect to the direction of applied electric field, as shown in Figure 2.4. When a molecule moves through the channel in response to the applied field, it has a finite probability to deflect to either side due to its Brownian motion (d_+ or d_- as indicated on Figure 2.4). Owing to the arrangement of the obstacles, changing the migration path in the lateral direction requires some finite amount of diffusion per unit time. Diffusion to the left (on Figure 2.4) requires a much longer diffusion distance d_- than diffusion to the right d_+. Therefore, the diffusion in the direction of d_- will be much less likely. Once the molecule diffuses a distance of d_+ (to the right on Figure 2.4), its diffusive motion is rectified by the obstacle preferentially in that direction. Since small molecules have larger diffusion coefficients than the larger molecules, the smaller molecules are more likely to be deflected in

the direction of d_+. Thus, the separation of molecules of different sizes occurs in a direction perpendicular to the direction of the electric field. Cabodi *et al.* [31] and Chou *et al.* [32] illustrated this technique independently and showed the separation of T2-and T7-DNA molecules, and XhoI-cut λ-DNA fragments (15 and 33.5 kbp), respectively. They fabricated their devices with photolithography and etching techniques on silicon-based substrate (for detailed fabrication steps, refer to [31] and [32]).

Even though each device successfully showed separation of the given DNA, there are a few shortcomings in this type of separation. First, the separation becomes less effective as the size of DNA becomes larger since large molecule is more likely to collide with the obstacles, stretching the coil and relaxing it back to the original coil conformation. Such a collision process would certainly upset the stochastic process by which the separation occurs [29]. It also should be noted that the slow diffusion of larger molecules requires the use of a low electrophoretic velocity, which would decrease the rate of separation with respect to time [29]. Lastly, this sieving method requires the use of a very dilute solution to prevent the steric intermolecular interactions that would affect the random motion of the DNA molecules.

2.5 Separation by post collision process

In 1992, Volkmuth and Austin [33] designed a micron-size post array (diameter of 1 μm) on a silicon wafer and showed the post collision process and size-dependent speed of DNA molecules for the first time. Since then, many research groups have conducted simulation studies of DNA separation by post collision [34–39]. In the last several years, we began to see actual experimental results of DNA separation by post collision process [7–10, 40–42].

Besides being a potential alternative for a new separation technique of large DNA, the post-collision process is quite relevant to my thesis. Therefore,

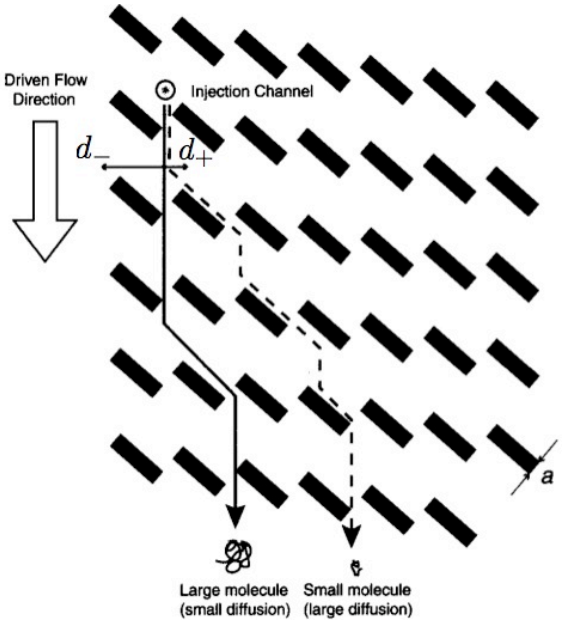

Figure 2.4: *Scheme for separating molecules by diffusion. Reprinted from [31].*

it is worth discussing the basic theory behind the separation process before showing some of the experimental results.

2.5.1 Theory: DNA colliding with a single obstacle

We consider a case in which a DNA molecule moving under a constant electric field collides with a single stationary obstacle. Such a collision process can be visualized as Figure 2.5. In this collision process, the so-called "rope-over-pulley collision", the DNA molecule collides with a post, hooks around it, making a U-shape conformation, and then eventually unhooks from it, returning to a random coil conformation.

In discussing the mechanism of this process, let us first make three assumptions. First, the radius of gyration of the molecule R_g is comparable or larger

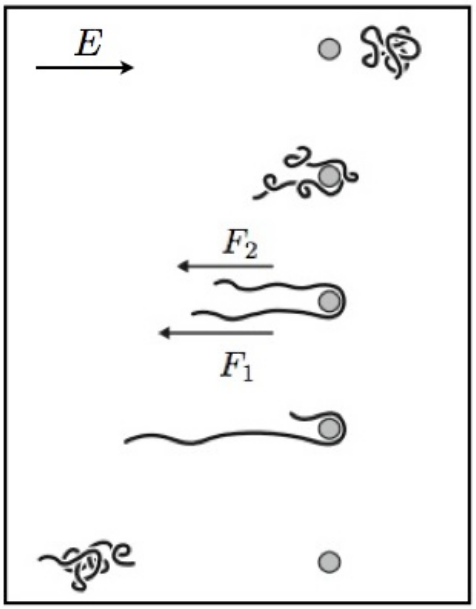

Figure 2.5: *Schematic of DNA colliding with a single post. Courtesy of Michel Gauthier.*

than the diameter of the obstacle d in order to avoid a roll-off collision [38]. Second, the motion by the electrodynamic force is much larger than the diffusive motion on scale of Kuhn length, which implies

$$\frac{q_k E l_k}{k_B T} >> 1. \tag{2.3}$$

Lastly, the DNA molecule follows the Rouse model so that the chain is freely draining.

When the DNA coil collides with the post, it deforms and extends into two arms around the post. The time for unraveling around the post to form the two arms scales like $L/\mu E$ [42]. For the simplicity, let us assume that the arms are fully extended so that the total arm length is the same as the contour length of the chain,

$$L = l_1 + l_2, \tag{2.4}$$

where l_1 and l_2 are the length of the longer arm and the length of the shorter arm respectively. The electric force acting on the longer chain (arm) is balanced by the electric force acting on the shorter chain and the total drag force, so that

$$\frac{q_k}{l_k} l_1 E = \frac{q_k}{l_k} l_2 E + \xi_c v, \tag{2.5}$$

where v is the curvilinear velocity of of the chain, which is the same as the change of the length of longer arm per unit time,

$$v = \frac{dl_1}{dt}. \tag{2.6}$$

Substituting Eq (2.6) into Eq (4.1) and rearranging the expression, the rate of change of the longer arm is

$$\frac{dl_1}{dt} = \frac{q_k E}{\xi_c l_k}(l_1 - l_2). \tag{2.7}$$

This differential equation has the solution

$$l_1(t) = \frac{L}{2} + \left(l_0 - \frac{L}{2}\right) \exp\left(\frac{2q_k E}{\xi_c l_k} t\right), \tag{2.8}$$

where $l_0 = l_1(t = 0)$. The total time for unhooking is the time when $l_1 = L$

$$t_{total} = \tau_o \ln\left(\frac{1}{2(l_0)/(L) - 1}\right), \tag{2.9}$$

where

$$\tau_o = \frac{\xi_c l_k}{2q_k E} \sim \frac{L}{\mu E}. \tag{2.10}$$

Finally, assuming that for each collision, l_0/L can take any value between $1/2$ and 1 with equal probability, the average unhooking time is given by

$$\langle t \rangle = \int_{\frac{1}{2}}^{1} \tau_o \ln \left(\frac{1}{2(\frac{l_o}{L}) - 1} \right) d\left(\frac{l_o}{L}\right) = \frac{\tau_o}{2}. \tag{2.11}$$

One thing to note is that Eq (2.9) diverges when $l_0 = L/2$. This is because this simple model neglects diffusion in the assumption of Eq (2.3). More rigorous models with inclusion of diffusion are found elsewhere, [5, 37]. However, the basic features of this simple rope-over-pulley model are preserved in more complex models.

The above result shows that the unhooking time is proportional to the chain length (molecular size) of the DNA molecule, thus demonstrating that the post collision process can be used for separation of DNA molecules by size.

2.5.2 Separation by post-collision: Micropost array

In the past few years, several research groups have reported separation of large DNA by the post-collision process. Doyle *et al.* and Minc *et al.* [7, 41] fabricated a micro-pillar array using the self-assembly of magnetic beads. For the fabrication, they first fabricated the microchannel by rapid prototyping and polydimethylsiloxane (PDMS) technology [43]. An emulsion of magnetic beads was then injected into the empty channel, and the magnetic field was applied perpendicular to the channel to align the beads into

a quasi-hexagonal array of stationary posts with average post diameter of $\approx$ 1 μm and average center-to-center post distance of $\approx$ 4 μm. They showed separation of λ-and T4-DNA within 3 minutes with the device.

Chan *et al.* [9] fabricated a high aspect ratio ($\approx$ 50) post array having diameter and spacing of $\approx$ 0.8 μm on Si wafer by photolithography and deep-reactive ion etching (DRIE) and showed separation of T4 (165 kbp) and EcoRI digested λDNA (21 kbp and 3-7 kbp) in 2 minutes.

Large DNA separations by micropost arrays made in PDMS have also been investigated by other groups [42, 44, 45]. The fabrication of PDMS post array is based on the soft lithography technique described by Xia and Whitesides [46]. Briefly, the PDMS prepolymer is poured onto the photolithographically patterned Si wafer mold, which contains the opposite image of channel and posts. The prepolymer is then cured, peeled from the master mold, and bonded with a cover slip to complete the channel structure. Ou *et al.* [45] reported a study of DNA electrophoresis with a hexagonal array of sparse PDMS posts ($\approx$ 1 μm post diameter with several microns of post spacing) while Randall and Dolyle [42] studied the electrophoretic interaction of large DNA with single isolated PDMS posts. Inatomi *et al.* [44] employed a more densely packed large PDMS post array in which the DNA motion is probably more preferably characterized by reptation rather than post-collision.

It is worth mentioning a few things about the PDMS post array. First, the fabrication of a PDMS post array is faster and more cost effective than a silicon-based post array since it does not require a repetitive cleanroom photolithography and etching processes. However, it is difficult to construct high aspect ratio posts with PDMS due to the mechanical instability of the elastomer. Secondly, PDMS is optically transparent so that it is ideal for observing and studying DNA electrophoresis under an optical microscope. Lastly, PDMS has a pervaporation problem; PDMS absorbs a fair amount of water, and the PDMS channel requires frequent supply of the buffer solution

during experiment.

2.6 Downsizing the post: Nanopost array

Micropost arrays have been investigated exclusively for the separation of large DNA well over several kilobase pairs (e.g. λ-DNA $\approx$ 49 kbp, T4-DNA $\approx$ 165 kbp) for which the radius of gyration of the molecule is comparable or larger than the size of the post. For more effective and frequent post collisions and a more efficient separation of DNA, it is desirable to decrease the size of the post further ($R_g \gg d$) to reduce the possibility of a roll-off collision, which produces a mobility independent of molecular weight [38,42], while maintaining control over the array density.

Kaji *et al.* [8] and Ogawa *et al.* [10] fabricated nano-pillar arrays using electron beam (EB) lithography and demonstrated the separation of large DNA molecules. For fabrication, a thin quartz substrate is sputter-coated with a Pt/Cr layer and then spin coated with EB resist. The EB resist is patterned into an array of a few hundred nanometer diameter holes using EB lithography. Nickel (Ni) is then electroplated into the array of holes. The remaining resist is removed, leaving an array of Ni pillars. The substrate is then etched with CF_4. After etching of the quartz substrate, Ni is removed by wet etching, and the substrate is bonded to a quartz top. The overall processing sequence is shown in Figure 2.6. Their post array consists of 500 nm diameter posts with 100 nm spacings (see Figure 2.7). Kaji *et al.* showed a separation of λ-DNA and T4-DNA within a few minutes while Ogawa *et al.* showed 10 kbp and 38 kbp DNA within a minute.

Recently, Chen *et al.* fabricated an even smaller pillar array, a pillar of 300 nm diameter, by nano-imprinting lithography (NIL). Figure 2.8 shows the fabrication of nano-pillars with NIL. Their master PDMS mold, which contains nanopillars, is made with EB lithography on Si wafer and subsequent

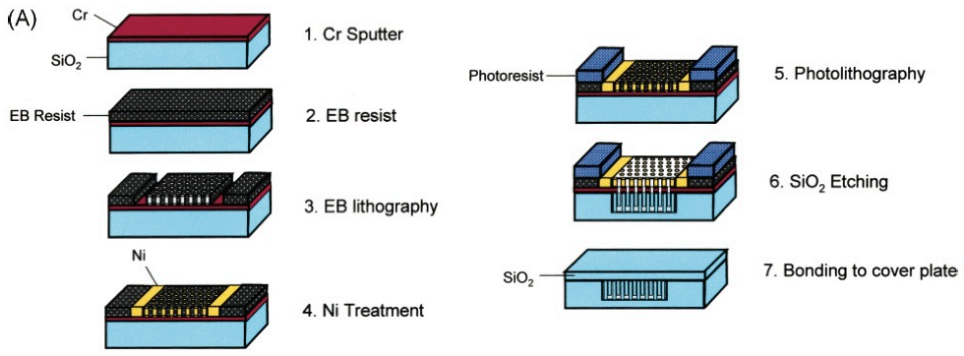

Figure 2.6: *Nanopillar fabrication steps with electron-beam lithography. Reprinted from [8].*

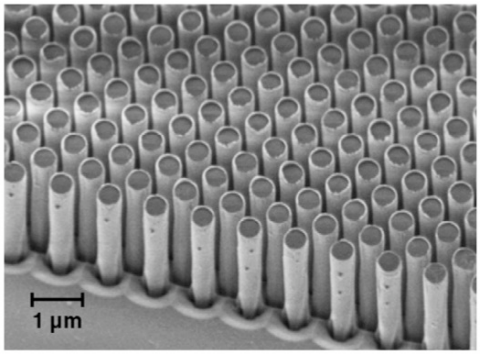

Figure 2.7: *Nanopillars fabricated by electron beam lithography. Reprinted from [10].*

PDMS replica method. First, the silica substrate is spin-coated with a tri-layer resist [47]. The substrate is then imprinted by the PDMS mold and exposed to UV light. The mold is removed from the sample after exposure, and the photoresist pattern is developed by dry etching. The Ni film is then deposited onto the substrate by evaporation, followed by a lift-off of the resist with acetone. The microfluidic channel is fabricated by photolithography over the area of the nanopillars. After developing the channel geometry, all of the patterns are transfered to the substrate by RIE. Finally the Ni film is removed, and the patterned substrate is bonded with a flat piece of PDMS. Figure 2.9 shows the SEM picture of the nanopillars. Using the device, they showed a separation of λ-and T4-DNA within 2 minutes [48]. One of the advantages of NIL over EB lithography is the reproducibility of the microchip without repetitive use of EB lithography, which is a costly and very slow process.

In addition to these reports, Chen *et al.* [49] more recently showed the fabrication of a dense nanopillar array using a nanosphere photolithography and used it for a simple single molecule study, though the fabrication method has a difficulty in controlling the nanopillar density.

2.7 ZnO nanowires as a post array

As described in the previous sections, micro- and nano-pillar arrays have shown to separate large DNA much faster than the PFGE. However, the post arrays fabricated with quartz and silicon require multiple cleanroom processes including an expensive and slow EB lithography step. Because of these complex fabrication processes and their costs, they are unlikely to replace gel electrophoresis in near future.

In this thesis research, ZnO nanowires (see Figure 2.10) are proposed and studied as novel point-size obstacles for DNA electrophoresis. ZnO nanowires,

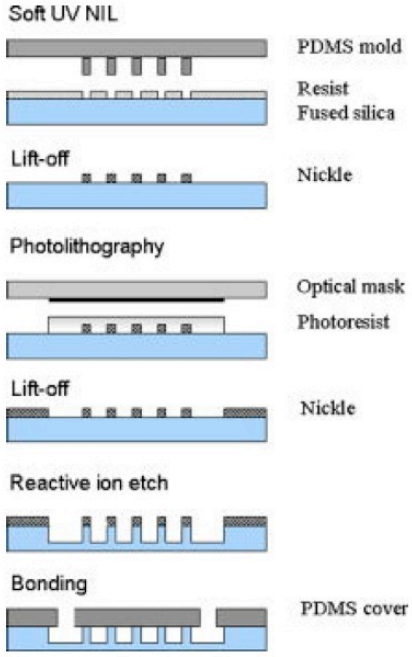

Figure 2.8: *Nanopillar microchip fabrication by nanoimprinting lithography. Reprinted from [48].*

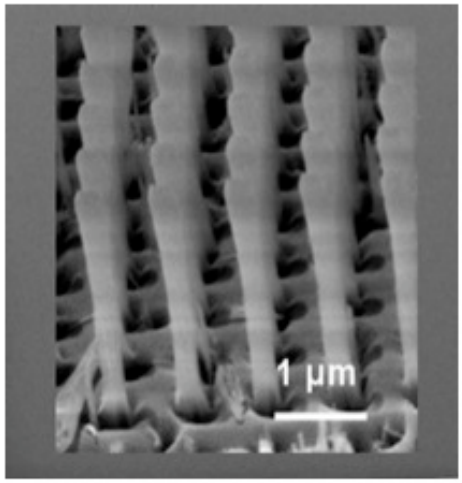

Figure 2.9: *Nanopillars fabricated by nanoimprinting lithography. Reprinted from [48].*

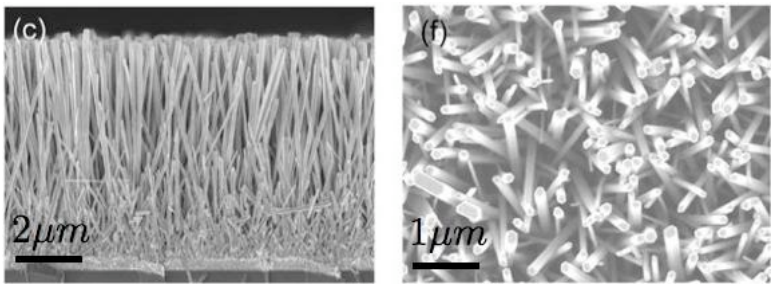

Figure 2.10: *Side view (left) and top view (right) of ZnO nanowires grown by simple solution chemistry. Reprinted from [52].*

a wide bandgap semiconductor material, have been studied for various applications in electronic devices including sensor, transistor, and solar cell [50]. However, it has never been proposed to use the morphology of the nanowires as a sieving matrix for DNA separation. There are several reasons we test ZnO nanowires as a nano-size matrix for DNA electrophoresis. First, ZnO nanowires can be grown by a simple aqueous solution chemistry, requiring only a few beakers, chemicals, and an oven [51]. Synthesis of ZnO nanowires is cheap and fast, requiring less than a single day; the growth of ZnO nanowires is through self-assembly, thus, it does not require expensive and time-consuming nano-scale patterning. Another advantage is that the synthesis of ZnO nanowires requires only mild temperatures ($\approx 90°$C), and thus, it can be grown on various substrates including glass. In addition, ZnO is naturally hydrophilic, eliminating the necessity of surface treatment.

The two main objectives of this thesis are to develop a robust and reliable protocol for the fabrication of a microfluidic chip in which ZnO nanowires are integrated in the microchannel and to conduct a fundamental study of DNA-nanowire interaction under an electrophoretic force using the developed chip.

Chapter 3

Device Fabrication

3.1 Synthesis of ZnO nanowires on a glass substrate

In this research, we study the interaction between ZnO nanowires and large DNA under electrophoretic motion, with the long-term goal of separating large DNA by size using ZnO nanowires as a sieving medium. The first stage of this research is to develop a robust protocol to embed ZnO nanowires into the microfluidic channel. The first thing we tested is to verify that the existing protocol for aqueous solution synthesis of ZnO nanowire is robust and reliable for our microchip platform.

ZnO nanowires were synthesized by slightly modifying the protocol developed by Greene *et al.* [51]. A soda lime glass was used as a substrate for this study. The substrate (2.4 cm x 4 cm) was first cleaned with an acetone/isopropanol/DI water (1:1:1 ratio) solution in an ultrasonic sonicator for 20 minutes. After sonication, the substrate was rinsed with DI water and dried with compressed air. Next, the substrate was wet with 100 μl of 5 mM

zinc acetate dihydrate in ethanol, evenly spread over the substrate surface, and dried in an oven at 90°C. This coating step can be repeated for a few times to ensure sufficient coverage of zinc acetate seeds on the substrate. The substrate was then annealed at 350°C for 30 minutes to convert the zinc acetate seeds into ZnO; at the end of the annealing process, the substrate surface is covered with a thin layer of ZnO nanoparticles. The ZnO nanoparticles seeded with this method have an average particle diameter of 5-20 nm and thickness of 3-5 nm [51]. ZnO nanowires were grown from the ZnO seeds by immersing the seeded substrate in an aqueous growth solution at 80°C that contains 16.8 mM zinc nitrate hexahydrate and 25 mM hexamethylenetetramine; the substrate was placed in the solution with the seeded side facing down to prevent the accumulation of ZnO precipitates from the solution and tilted at $\approx 45^{\circ}$ to prevent the accumulation of air bubbles on the substrate surface, which would result in non-uniform nanowire growth. After about four hours in the growth solution, the growth of nanowires slows down due to the depletion of the precursors in the solution. The growth of the nanowires can be continued by introducing the substrate into a fresh growth solution. We define four hours in the growth solution as one cycle and replace the growth solution after each cycle for further growth. After the growth of nanowires, the substrate was removed from the solution, rinsed thoroughly with DI water, and dried with compressed air.

Figure 3.1-a shows a digital camera image of ZnO nanowires (bluish part) grown on a glass substrate following the protocol as described. To check the morphology of the nanowires, the sample was examined under a scanning electron microscope (SEM) at the Characterization Facility at the University of Minnesota. Figure 3.1-b shows the SEM image of the ZnO nanowires grown for one cycle. It reveals the dense array of ZnO nanowires with pillar diameter and pillar spacing of roughly 100 nm. Also, a profilometer measurement shows the height of the nanowires to be ≈ 1 μm after one cycle of growth.

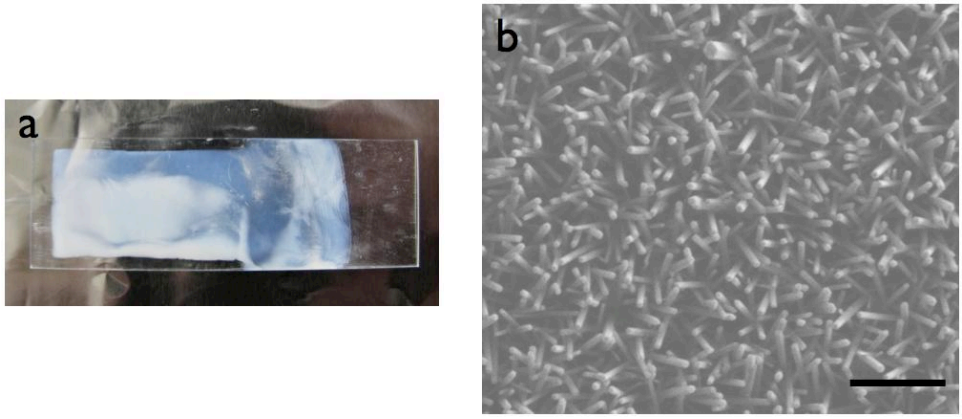

Figure 3.1: *a) Digital camera image of ZnO nanowires grown on a glass substrate. b) SEM image of the nanowires. The scale bar is 1 μm.*

Having showed that our nanowire synthesis protocol is robust, next task was to develop a method to selectively synthesize the nanowires inside the microchannel, and this will be discussed in the following sections.

3.2 Fabrication of the microchannel by wet etching

A micro-fluidic channel was fabricated on a glass substrate by selective wet etching. Glass is the preferred choice of substrate material for its optical clarity and good electrical insulation. A chrome-photoresist-coated glass plate (NANOFILM) was used as a starting material. First, the photoplate was selectively exposed to UV-light (UV-400 lamp) for 15 seconds using a chrome mask that contains multiple shifted-T channel geometries (Figure 3.2). Then, the plate was developed with a photoresist developer (Microposit 351, Rohm&Haas) for 40 seconds, making shifted-T channel patterns with the photoresist. Next, the substrate was immersed in a chrome etcher (CR-12S, Cyantek Corp.) for two minutes to selectively remove the chrome

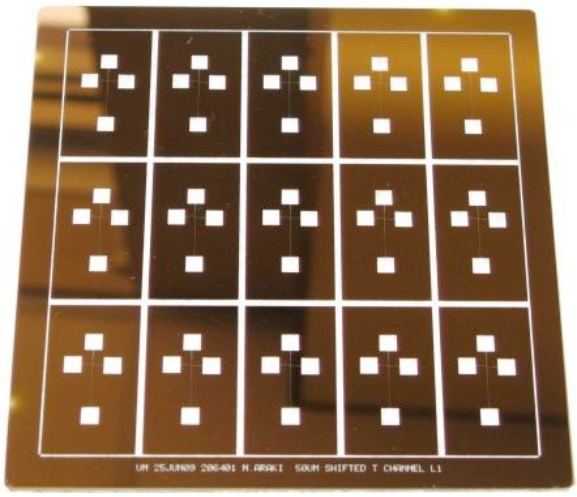

Figure 3.2: *5 inch by 5 inch Cr mask that contains multiple shifted-T channel geometries.*

film. After the selective etching of chrome, the plate was rinsed with acetone to remove the photoresist and soaked in a sulfuric acid bath at 115°C for 30 minutes to remove any organic contaminants such as the resist residues from the substrate surface. The substrate was then immersed in a buffered oxide etcher (BOE, J.T. Baker) for selective etching of the glass surface; the etching rate was measured as $\approx$ 0.3 μm per minute. It is worthwhile to remember that this is wet etching of an amorphous material, thus the etching is isotropic. The deeper the channel is etched, the wider the channel becomes. After the etching, the substrate was soaked in the chrome etcher to remove the remaining chrome film and rinsed with DI water. The plate was finally sliced into small pieces, each having $\approx$ 2.4 cm x 4 cm x 0.23 cm dimension and containing one shifted-T channel geometry. Figure 3.3 shows the sequence of the fabrication steps, and Figure 3.4 shows the surface profile of the channel by profilometer.

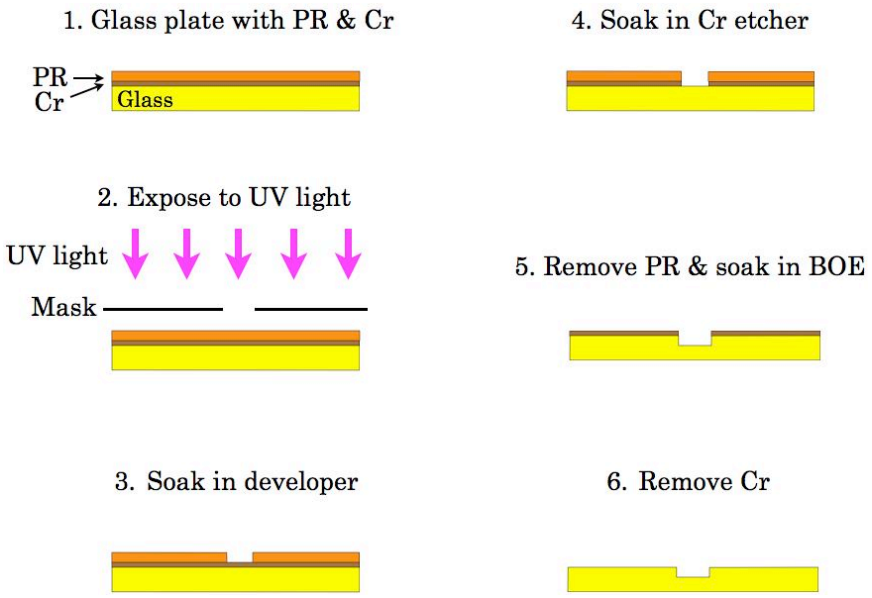

Figure 3.3: *Processing steps for making a microchannel on glass substrate.*

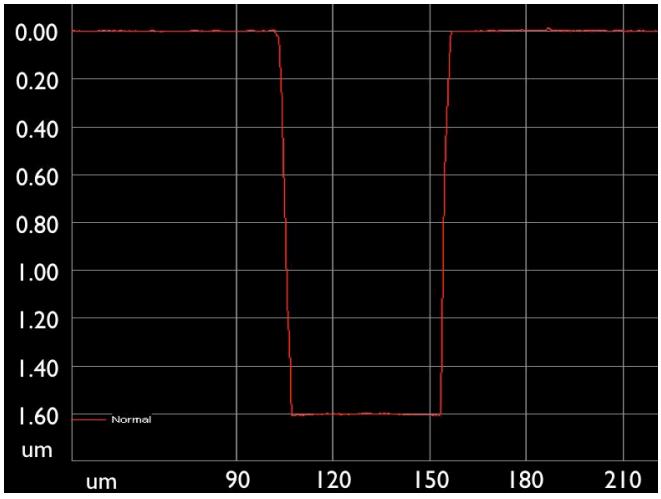

Figure 3.4: *Channel profile by surface profilometer measurement. The channel is etched for five minutes by BOE.*

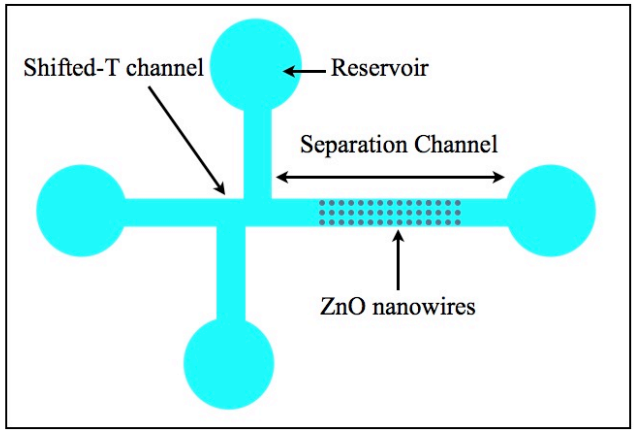

Figure 3.5: *Schematic of shifted-T microchannel with nanowires in the separation channel.*

3.3 Selective growth of ZnO nanowires in the channel

Figure 3.5 shows a rough sketch of the shifted-T microchannel with nanowires in the separation arm. The channel has a width of ≈ 50 μm and a depth of ≈ 2 μm, and the length of the separation channel is 1 cm. The nanowires are only in the separation channel, and any nanowires present outside the separation arm could cause problems in device integrity. Thus, it was necessary to develop a technique to grow ZnO nanowires selectively on the substrate with micron scale resolution. In this section, we discuss our method to synthesize a uniform array of nanowires accurately in the separation arm.

3.3.1 Seeding inside the microchannel

For device integrity, especially for the purpose of a future separation experiment, it is important to have a homogeneous array of nanowires across the channel, and uniform seeding is one of the most important steps for achieving

the uniform nanowire array.

As discussed in a previous section, the glass substrate with microchannel geometry was first cleaned with an acetone/isopropanol/DI water solution in a sonicator. Next, the substrate was wet with 100 μl of seed solution, spread evenly over the substrate surface, and then dried. Here, we found that the drying process is the crucial step in achieving a uniform seeding across the channel. Figure 3.6-a shows the nanowires for which the substrate was dried slowly with room temperature and followed by the subsequent synthesis steps; the non-uniform nanowire morphology is easily seen across the channel. Figure 3.6-b shows the case in which the substrate was dried at 90 °C in an oven. It shows an improvement compared to the one dried at room temperature, but it still shows some dense nanowire regions around the channel sidewall. This is most likely due to the meniscus formation around the sidewalls during drying process, with the high concentration meniscus liquid drying last. Based on this hypothesis, we tested drying the substrate at the maximum temperature of our oven, ≈ 220°C, and the result (Figure 3.6-c) shows the most homogeneous growth among the three different temperatures, minimizing the effect of meniscus on the sidewalls. Thus, it appears that the high temperature flash drying works best for our purpose, and all subsequent work uses this method. After seeding, the substrate was annealed on a hot plate at 350°C for 30 minutes (as described in ∮3.2) to convert the zinc acetate layer into ZnO.

3.3.2 Patterning the nanowires with photolithography

Achieving a uniform coating over the substrate surface with ZnO nanoparticles, we are now ready to pattern the seeds for selective growth of nanowires. Figure 3.7 shows the developed process sequence for the patterning of ZnO nanowires. All the photolithography steps were done in the Nanofabrication Center (NFC) at the University of Minnesota.

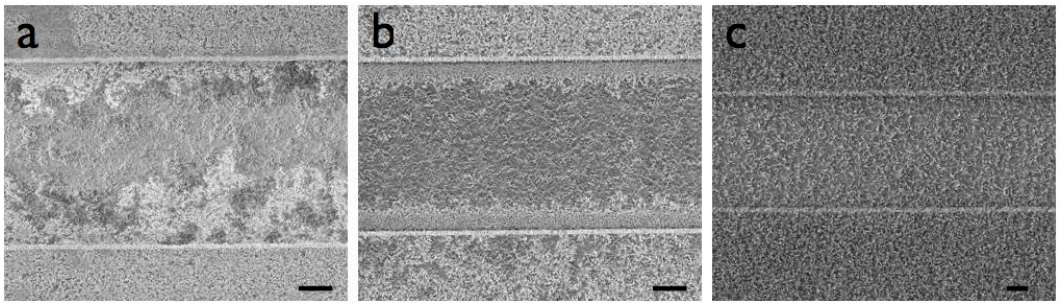

Figure 3.6: *After coating with seed solution, the substrates were dried at a) room temperature, b) 90 °C, and c) 220 °C, followed by the subsequent synthesis steps.*

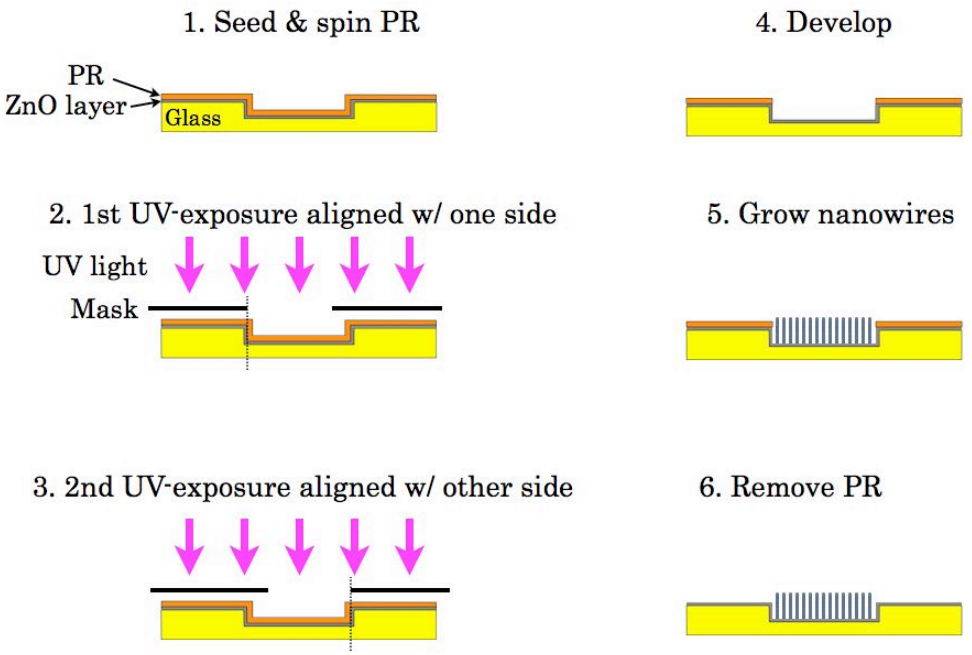

Figure 3.7: *Processing steps for patterning ZnO nanowires.*

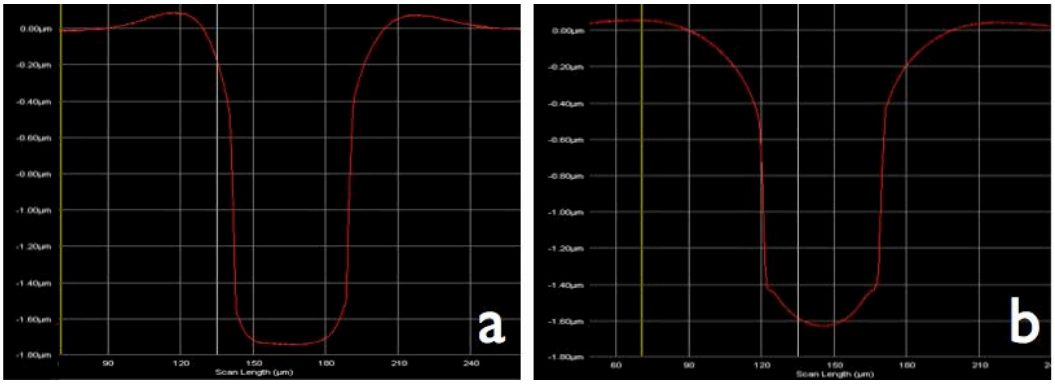

Figure 3.8: *a) The photoresist is spun at 5000 rpm with acceleration of 5000 r/s. b) the photoresist is spun at 2500 rpm with acceleration of 250 r/s*

First, the seeded substrate was spin-coated with a positive photoresist (S1805, Shipley) for 30 seconds at 5000 rpm, resulting in a resist thickness of about 0.6 μm. Keep in mind that we are spin-coating over the patterned surface, not on a flat surface, and the thickness profile of the photoresist inside the channel trench is not uniform, as seen in Figure 3.8. Because of the presence of the channel sidewall, the photoresist becomes thicker as it gets closer to the sidewall. This effect is more pronounced if the spin speed is decreased; compare Figure 3.8-a for 5000 rpm with fast acceleration and Figure 3.8-b for 2500 rpm with slow acceleration. The non-uniform resist thickness across the channel becomes problematic when we develop the photoresist pattern, since the thinner part will be developed faster than the thicker part. After the resist coating, the substrate was soft-baked at 115 °C for 2 minutes to evaporate the resist solvent residue.

Next, the resist-coated substrate needs to be aligned with respect to the chrome mask to selectively expose the separation channel to UV light. Remember that the channel was made by isotropic wet etching and that it is difficult to have the width of the channel to be exactly the same as the width of the strip pattern on the mask. To circumvent this problem, we employed a mask that has a smaller strip width than the channel width and did a

double exposure; first, the mask was aligned with respect to one side of the channel wall and exposed to UV light for 10 seconds, and then the mask was aligned with respect to the other side of the channel wall and exposed to UV light for 10 seconds again, as shown in Figure 3.7. Note that the alignment was done using Karl Suss Mask Aligner, MA-6, that has a maximum mechanical resolution of 0.1 μm and that the 20 second exposure is long enough to fully convert the exposed photoresist to a developer-soluble state; a positive photoresist becomes soluble to the developer after exposure to UV light.

Following the UV exposure, next step is to immerse the substrate in a photoresist developer to remove the resist on the exposed area. Here, it is important to remember that ZnO is amphoteric, meaning that it is soluble in both acid and base, and all the positive photoresist developers available in the NFC are strong basic solutions with pH of around 13. Thus, soaking the seeded substrate in the normal developer dissolves the ZnO seeds on the substrate fairly quickly and thus spoils the sample. To avoid this problem, the developer (Microposit 351) was diluted to one seventeenth of its original concentration by DI water (10 ml of original Microposit 351 developer plus 170 ml DI water), and the substrate was developed slowly with the very dilute developer solution. The substrate was held on a sample holder and gently placed in the developer, and there was no agitation of the sample or swirling of the solution during developing. Soaking in the developer for too short of a time would result in underdeveloping (Figure 3.9-a), and soaking too long would dissolve both photoresist and ZnO seeds (Figure 3.9-b); due to the non-uniform resist thickness in the channel, the resist starts developing from the center of the channel. After trial and error, the optimum developing time with our process parameters was found to be 2.5 minutes. After removing from the developer, the substrate was rinsed in a DI water bath for 30 seconds and dried with nitrogen gas. After the photolithography process, the substrate is covered with photoresist except over the separation

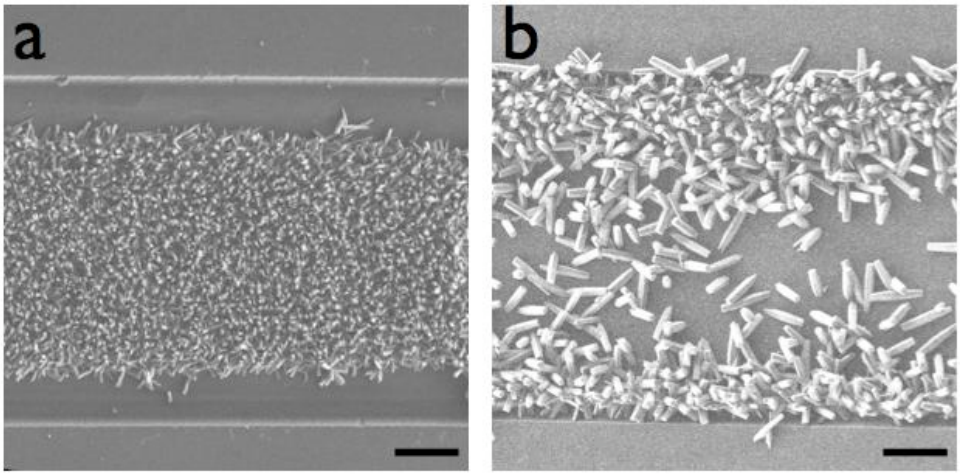

Figure 3.9: *a) An underdeveloping case. Photoresist around the side walls was not fully removed, thus preventing nanowire growth. b) An overdeveloping case. The developer etched away most of the ZnO seeds on the center of the channel.*

channel.

Next step is to place the substrate in the nanowire growth solution. During growth, the photoresist functions as a sacrificial layer to prevent the growth of nanowires. Nanowires are able to initiate growth only from the ZnO seeds on the separation arm directly in contact with the growth solution. After the growth of nanowires, the substrate was removed from the solution, cleaned with DI water, rinsed with acetone to lift off the resist, rinsed again with DI water, and then dried with air. The patterned nanowires inside the microchannel are shown in Figure 3.10.

3.4 Nanowire density control

The long term goal of this research program is to separate large DNA by size using ZnO nanowires as a sieving medium. It is crucial that the spacing

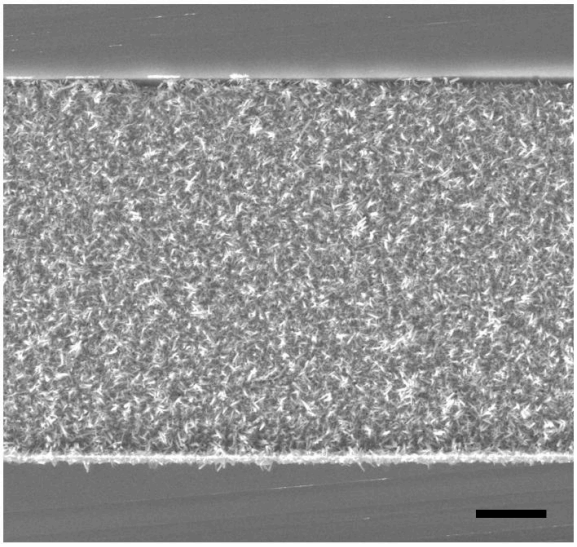

Figure 3.10: *SEM image of ZnO nanowires synthesized inside the 50 μm wide channel. The scale bar is 10 μm.*

between the nanowires is large enough for large DNA to move through. As shown in §3.2, the nanowires synthesized with 5 mM seed solution are quite densely populated, and it may not be the optimum density for large DNA fragments. It will be advantageous to have a facile method to control the nanowire density. Here, we show that the nanowire density can be easily controlled by changing the concentration of zinc acetate in the seed solution; the clean glass substrates were coated with 100 μl of seed solutions of different concentrations, annealed, and then immersed in a growth solution with the previously described parameters. The resultant nanowires were examined under the SEM. Figure 3.11 shows the nanowires seeded with $\approx$ 1 mM seed solution and $\approx$ 0.25 mM seed solution respectively. The pictures clearly indicate that the density of nanowires can be controlled by changing the concentration of the seed solution. It is also worthwhile to mention that the density can be controlled by changing the number of seeding cycles as well.

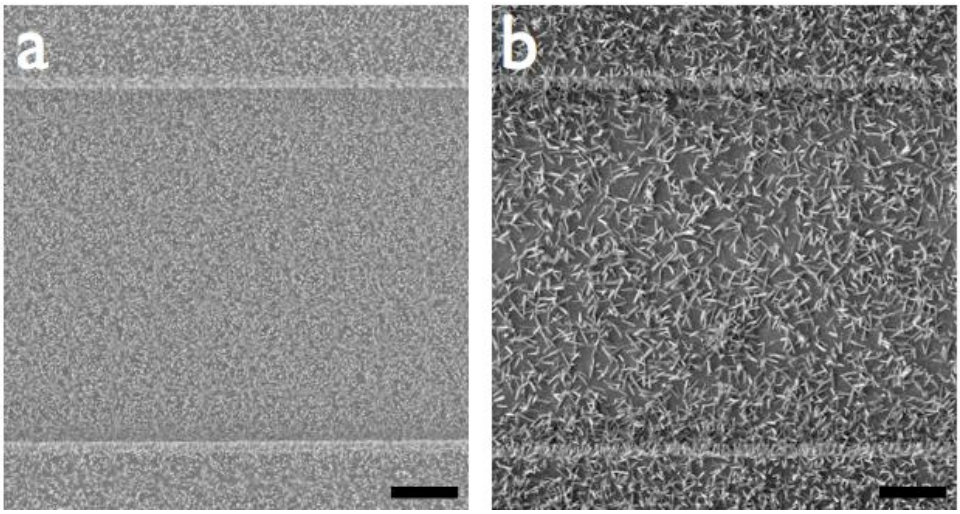

Figure 3.11: *Nanowires seeded with a) 1 mM seed solution. b) 0.25 mM seed solution. The scale bar is 10 μm.*

This simple method is directly applicable to the patterned nanowires inside the channel. Figure 3.12 shows the patterned nanowires in the channel seeded with seed solutions of three different concentrations, resulting in a very sparse array of nanowires (a), a moderate density of nanowires (b), and a dense array of nanowires (c), proving that the density of the imbedded nanowires is easily controlled by the seed solution.

3.5 Sealing the chip with UV curable adhesive

The previous sections discussed the method to embed the nanowires inside the channel. The last step of the chip fabrication is the sealing of the channel. The reservoirs for the injection of buffer solution, DNA, and electrodes were made on the substrate by drilling holes using a diamond drill bit prior to sealing. After making reservoirs on the substrate, the channel is ready to be

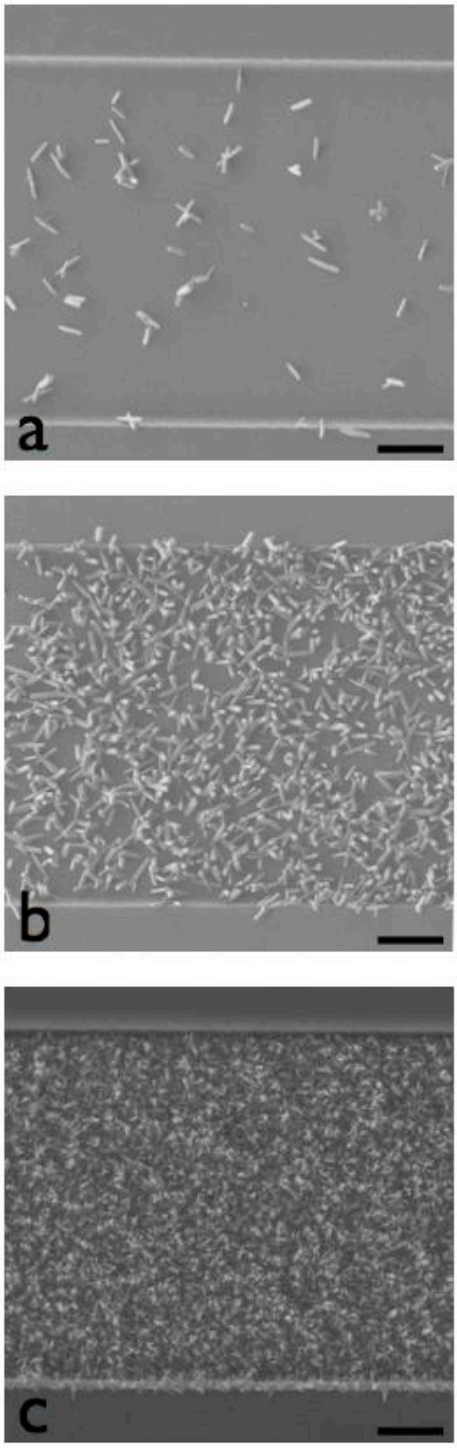

Figure 3.12: *Patterned nanowires with three different densities. The scale bar is 10 μm. The seed solution concentrations used are $\approx$ 0.2 mM for (a), $\approx$ 0.25 mM for (b), and $\approx$ 1 mM for (c).*

sealed. To be able to focus with the microscope objective lens of up to 100x, the substrate needs to be sealed with a thin material. We used an UV-curable adhesive (NOA 81, Norland Products) spun on a No.1 coverslip as a sealing material. NOA-81 is a great material choice for microfluidic device sealing because of its excellent adhesion to glass, optical transparency, resistance to solvent swelling, and hydrophilicity [53].

First, a clean coverslip was treated with an oxygen plasma (PDC-32G, Harrick Plasma) for three minutes to enhance the wetting property of the glass surface. Then, the NOA 81 was spin-coated on the coverslip at 1200 rpm for 30 seconds; however, the spin coating does not spread the viscous NOA-81 over the substrate surface evenly, always leaving small bumps (edge bead effect) around the surface edges; the edge bead effect becomes more pronounced when the viscosity of the spun material increases or the shape of the substrate is non-circular [54, 55]. To remove those edge beads and make a flat NOA 81 film, the coverslip spun with NOA 81 was sandwiched between two flat PDMS slabs and then brought under UV light for three minutes to cure. After curing, the PDMS slabs were peeled from the coverslip, leaving a flat NOA 81 film on the coverslip. The coverslip with the NOA 81 film was then brought gently in contact with the channel substrate for sealing.

Chapter 4

DNA electrophoresis with nanowires

4.1 Electrophoresis with a sparse nanowire array

The long term objective of this research project is to separate large DNA fragments by size using ZnO nanowires as a sieving medium. This chapter discusses our experimental study and analysis of electrophoretic interaction between a large DNA (λ-DNA) molecule and a single isolated nanowire. Our main goal is to verify the theoretical prediction [56] that the hooking time of DNA around the point size obstacle under electrophoretic force is exponentially dependent on the impact parameter, b, which is the distance between the center of mass of DNA and post at impact, measured perpendicular to the field (See Figure 4.1). To do that, we need to be able to record an isolated interaction between DNA and a nanowire. Thus, we used a very low concentration of DNA solution to focus on the motion of a single DNA molecule without being disturbed by other neighboring molecules, and also we em-

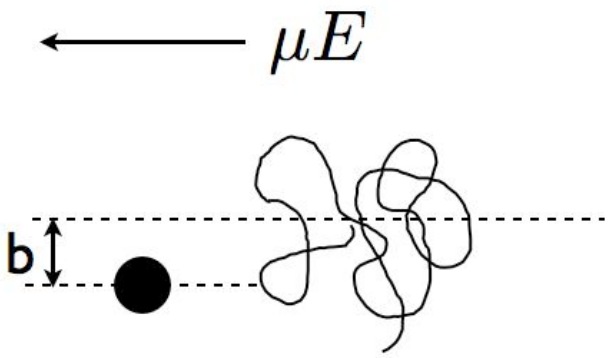

Figure 4.1: *Impact parameter measurement.*

ployed a very sparse array of nanowires so that the DNA collide and hook around a single nanowire instead of reptating through the nanowire matrix, which might be the case if the nanowires are dense. It is also important that the spacing between the nanowires is large enough so that the DNA conformation at the impact is not affected by the previous DNA-nanowire interaction. Figure 4.2 shows the type of the nanowire array used in this experiment. The nanowires have a diameter of 200 - 300 nm and a spacing of ≈ 10 μm. Note that the nanowires are not vertical and are tilted in random directions. This will make the accurate measurement difficult if the DNA has a freedom in Z-axis (vertical) motion. The radius of gyration of λ-DNA is ≈ 0.7 μm, thus we set the depth of the channel $\approx$1.5 μm so that the DNA is confined in the vertical movement.

4.1.1 Buffer solution and dyeing of DNA

The TBE (Tris/Borate/EDTA) buffer is one of the most common buffer solutions used in DNA electrophoresis, and the standard buffer concentration used for gel electrophresis is normally denoted as 1x. The 1x TBE solution consists of 89 mM tris base, 89 mM boric acid, and 2.8 mM ethylene-diamine-tetraacetic acid (EDTA). Tris base and boric acid keep the pH constant under

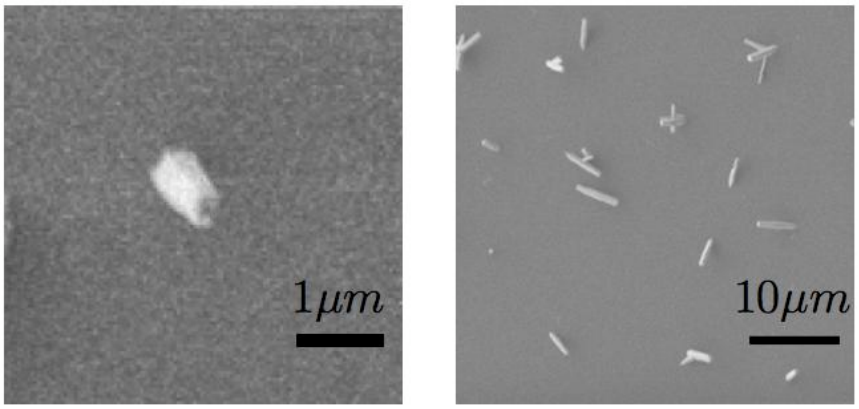

Figure 4.2: *SEM image of a sparse nanowire array used in the experiment. Note that the nanowires are tilted, not vertical.*

the applied electric field. EDTA is added to deactivate metal-dependent enzymes that might damage DNA. The pH of TBE buffer is around 8.3. ZnO is amphoteric, thus it reacts with either acid or base. In fact, soaking the ZnO nanowires in a regular TBE buffer solution results in fairly quick dissolution of nanowires, as shown in Figure 4.3. The solubility of an amphoteric material is normally minimized by adjusting the pH of the liquid medium at the isoelectric point of the material; by definition, isoelectric point is the pH value at which a molecule or material carries no surface charge (zero zeta potential). The reported isoelectric point of ZnO is between 9.2 - 9.5 [57,58] varying slightly from article to article.

For this research, we chose to use TB (Tris/Borate) buffer with its pH adjusted to 9.2. The pH of the buffer solution was adjusted by decreasing the amount of boric acid; it consists of 89 mM tris base and 15 mM boric acid. With the adjusted pH, the nanowires were stable in the buffer solution for up to two days. In addition to these components, polyvinyl pyrrolidine (PVP, 0.7 g/liter) was added to the buffer solution to reduce the electroosmotic flow on the glass surface, and 50 mM dithiothreitol (DTT) was added to reduce the photobleaching of the DNA-dye compounds.

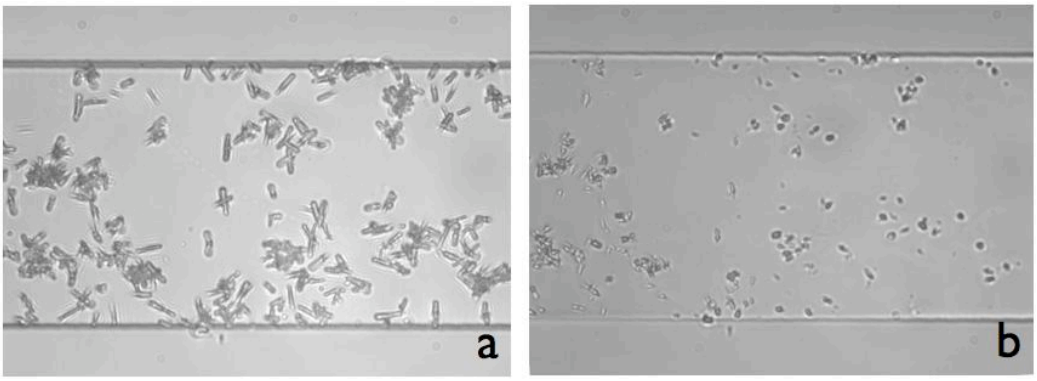

Figure 4.3: *a) Nanowires before soaking in the 1x TBE buffer. b) Nanowires after soaking in the buffer for 90 minutes.*

λ-DNA was dyed with YOYO-1 (Molecular Probes) at the ratio of one YOYO-1 molecule to ten base pairs of DNA. YOYO-1 is a fluorescent intercalating dye that absorbs light of wavelength 475 nm and emits light of wavelength 540 nm [59]. The DNA-dye solution was prepared as ≈ 0.3 μg/ml.

4.1.2 Injection of DNA and data collection

The microfluidic chip was mounted on a movable stage of an inverted microscope (DMI 4000B, LEICA). A volume of 150 μl of TB buffer was added to reservoirs A, B, and C as labeled in Figure 4.4. A volume of 150 μl of dyed λ-DNA solution of very low concentration (≈ 0.3 μg/ml) was added to reservoir D. A platinum electrode was inserted in each reservoir as shown in Figure 4.5. These electrodes were connected to a high voltage power supply (HVS448, LabSmith), and the electric field on each arm of the shifted-T is controlled by LabView (National Instruments). An electric field of 5 V/cm was applied in the arm D that contains a very sparse nanowire array, and DNA move from reservoir D toward reservoir A with a continuous flow through the sparse nanowire array. The movement of DNA was observed by epifluorescence un-

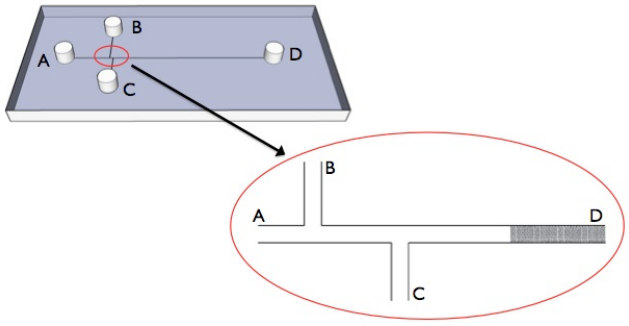

Figure 4.4: *Geometry of shifted-T channel.*

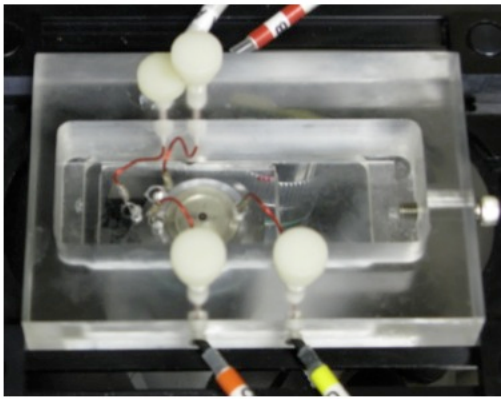

Figure 4.5: *Picture of the assembled chip with electrodes inserted in the reservoirs.*

der a 100x oil immersion objective lens by illuminating the channel with a metal halide light (Leica) filtered for the excitation wavelength of YOYO-1. The motion of DNA through the nanowire array was recorded by an EM-CCD camera (Photometrics) and PM Capture-Pro at the recording rate of 25 frames per second. Fifteen movies of 32-second duration (800 frames) were taken for the electric field strength of 5 V/cm. The same process was repeated for the electric field strength of 10 V/cm and 20 V/cm.

4.2 Basic hooking conformation

Many research groups studied the DNA conformation during collision using a silicon or PDMS post that has a post diameter of 1-2 μm and categorized the DNA-post collisions into several types depending on the conformation of two arms of the chain during collision. The most well known ones are J, U, X, and W collisions [60]. The schematic of these collisions are shown at the top of Figure 4.6; the J-collision is the one in which the molecule assumes J-shape configuration at the onset of unhooking from the post (short arm starts retracting from the post) whereas for the U-collision, the molecule makes a U-shape configuration at the onset of unhooking. The X-collision is the one in which the longer arm is still extending while the shorter arm starts retracting; in other words, the head of the longer arm has a kink at the maximum extension.A W-collision is a collision in which both ends of the chain are located on the same side of the obstacle during hooking. Figure 4.6 compares the U, J, and X-collisions of λ-DNA observed with 1 μm diameter silicon post (from Dorfman's lab) and those collisions observed with our nanowires. For collisions with a 1 μm silicon post, it is easy to observe two arms extending from the post and recognize the shape of U, J, and X configurations. In the case of the collision with a nanowire, it is more difficult to distinguish two arms extending from the nanowire since the two arms overlap due to the small nanowire diameter. For hooking with a nanowire, the molecules form a skewed shape of U, J, or X conformation in many occasions, as shown in Figure 4.6. The conformation change during collision will be discussed in more detail in a later section.

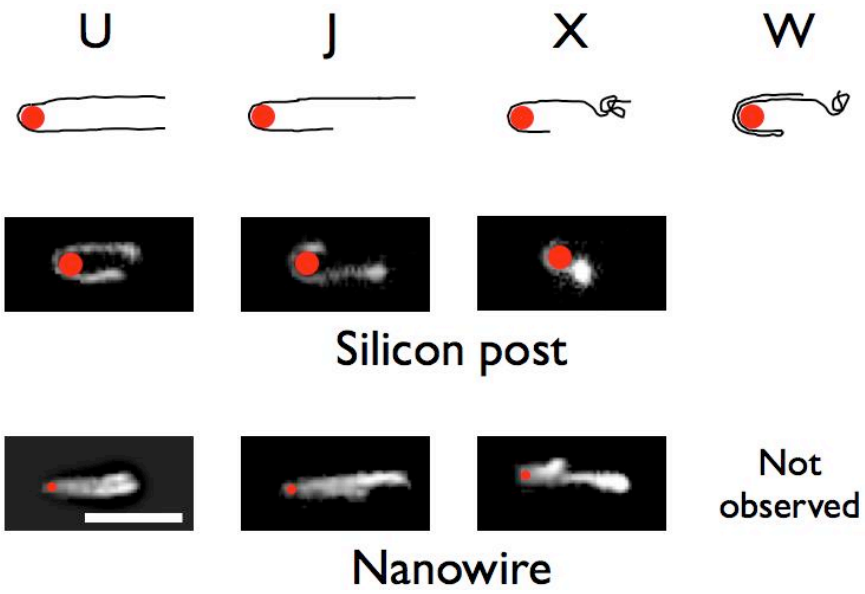

Figure 4.6: *Schematic of U, J, X, and W-configuration and the observed U, J, and X-collisions of λ-DNA with a 1 μm diameter silicon post and nanowire. The scale bar is five micron.*

4.3 Hooking time measurement: Data processing

The DNA movies taken by the PM Capture-Pro were read by the molecule tracking GUI developed by Michael Meloche and Dan Olson in Dorfman's group. First, all the images were filtered to remove the background noise, and then the images were converted from gray-scale intensity images into binary images; these binary images were used to define the area occupied by the molecule. The center of mass of DNA was calculated by finding the first moment of the post-filtered DNA image from the intensity distribution. We define the x-coordinate as the direction of the electric field and the y-coordinate as transverse to the electric field direction. The y value of the centroid of the nanowire was calculated by finding the transverse nanowire

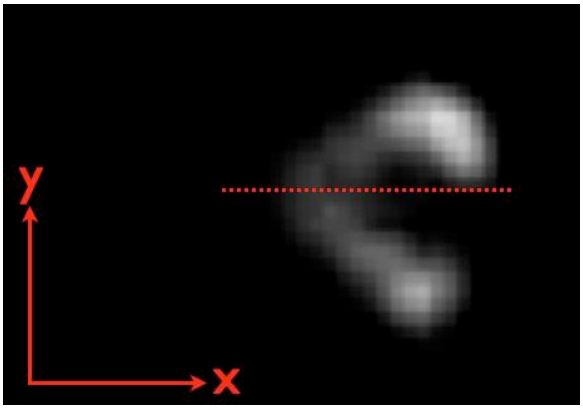

Figure 4.7: *Finding y value of centroid of nanowire from the axis of hooking pivot.*

location of DNA hooking which is equivalent to the y-axis displacement of the hinge point of DNA molecule (Figure 4.7). The impact parameter was then found as the difference between the y value of the center of mass of the molecule at impact and the y value of the center of mass of the nanowire. The hooking time is defined as the time it takes from impact to completely unhook around the nanowire. The hooking time of 100 molecules were collected for each electric field strength and the hooking time was plotted against b/R_g, where $R_g = 0.7$ μm for λ-DNA.

4.4 Conformation during collision

Figure 4.8 compares the conformation change of DNA during collision for small values of b/R_g (< 0.1) at impact. Figure 4.8-a), c), and e) are for long-lived collisions for $E = 5$ V/cm, 10 V/cm, and 20 V/cm respectively. Notice that all three collisions have a clear U-shape conformation at some point during hooking. It is also seen that the DNA at 10 V/cm and 20 V/cm are a lot more stretched than the molecule at 5 V/cm. This indicates that at $E = 5$ V/cm, the contribution from the diffusive motion is more significant

and the molecule is less stretched by the electric force than the other two electric field strengths. The pictures also show that the molecule is stretched to the length of ~ 10 μm even at $E = 20$ V/cm. This is still much smaller than the contour length of λ-DNA (21μm [61]). All of the long-lived collisions observed in our movies are classified as U-collisions.

Figure 4.8-b), d), and f) show the conformational change during the short-lived collisions for small values of b/R_g (< 0.1) for $E = 5$ V/cm, 10 V/cm, and 20 V/cm respectively. For collisions b) and d), we see (though it is not as clear for d)) the presence of a kink at the end of the longer arm when the short arm starts to retract. Therefore, it is appropriate to categorize them as X-collisions. For collision f), it seems that the chain is well stretched into two arms with one arm slightly longer than the other arm at the maximum extension. Thus, it is categorized as a J-type collision.

Figure 4.9-a), b), and c) show the conformational change of DNA for large values of b/R_g (≈ 1) for $E = 5$ V/cm, 10 V/cm, and 20 V/cm respectively. All three collisions show the presence of a kink at the end of the longer arm at the onset of unhooking, thus they are all categorized as X-collisions.

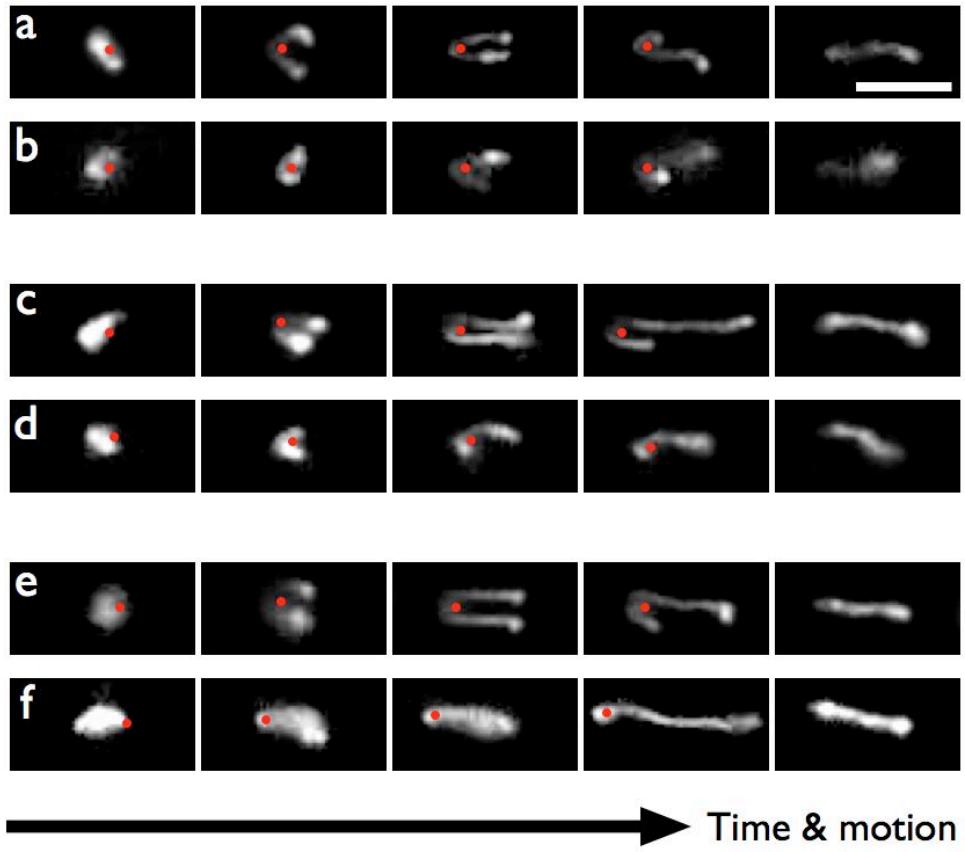

Figure 4.8: *Head-on collision with a) short hooking time with E = 5 V/cm. b) long hooking time with E = 5 V/cm. c) short hooking time with E = 10 V/cm. d) long hooking time with E = 10 V/cm. e) short hooking time with E = 20 V/cm. f) long hooking time with E = 20 V/cm. The red dot shows the location of the nanowire for clarification. The scale bar is 5 μm.*

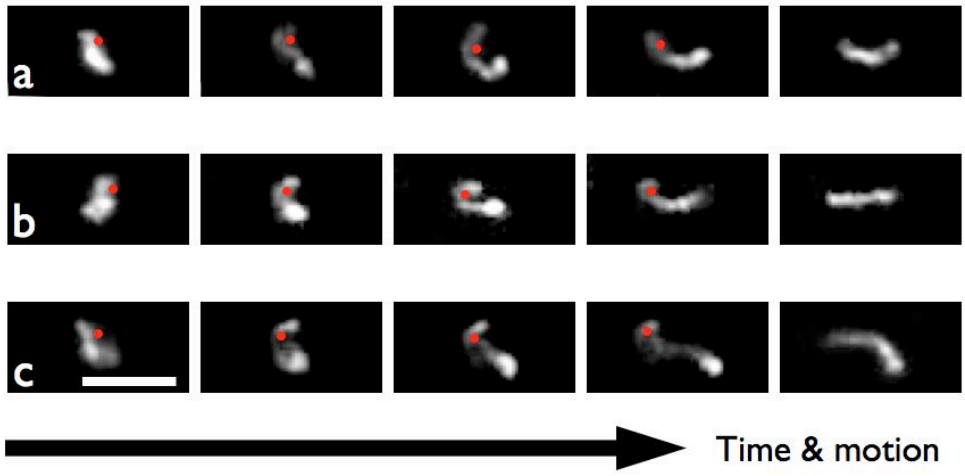

Figure 4.9: *DNA conformation change for large values of b/R_g for the electric field strength of a) 5 V/cm b) 10V/cm c) 20 V/cm.*

4.5 Analysis of hooking time

Previously, Sevick and Williams [56] conducted a simulation study of the collision of DNA with a point size obstacle. They found that the hooking time of DNA around a point size obstacle follows a universal form

$$\langle t_H \rangle = \frac{\eta N}{\lambda E} f\left(\frac{b}{R_g}\right), \tag{4.1}$$

with fluid viscosity η, a degree of polymerization N, and an effective charge per unit length λ. Their simulation shows that f becomes a simple exponential provided b is less than a few R_g. They do not discuss any special relevance for the exponential behavior. They only claim that their simulation study shows that the behavior is well fit by an exponential function. We do not intend to discuss the detail of the formula either; we are only interested whether our collected data points follow an exponential behavior.

Figure 4.10 shows the plots of the hooking time, t_{H}, versus b/R_g and $\ln(t_{\mathrm{H}})$

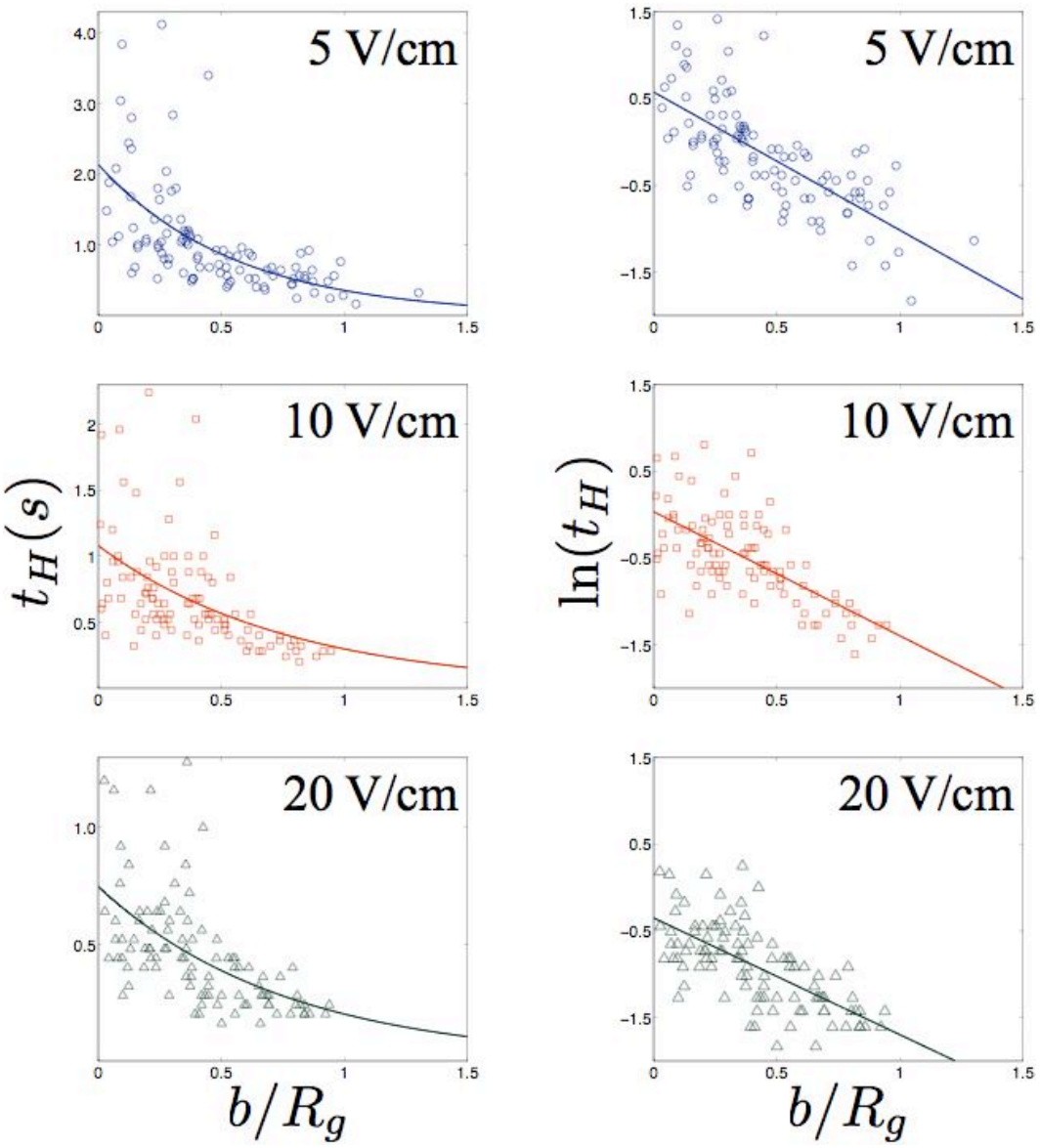

Figure 4.10: *Plots of hooking time v.s.* b/R_g *and* $\ln(t_{\mathrm{H}})$ *v.s.* b/R_g *for the electric field strengths of 5 V/cm, 10 V/cm, 20 V/cm. The plots for* t_{H} *v.s.* b/R_g *are fitted with a simple exponential function, and the semi-log plots are fitted with a linear function.*

versus b/R_g for three different electric field strengths, 5 V/cm, 10 V/cm, and 20 V/cm obtained in our experiment. The plots does seem to show the exponential dependence of hooking time on b/R_g. It is also seen that the maximum hooking time observed in the experiment is linearly (or sub-linearly) dependent on the electric field strength, with $\approx$ 4 seconds for 5 V/cm, $\approx$ 2 seconds for 10 V/cm, and $\approx$ 1 second for 20 V/cm.

The plots show the small scattering of data points for large values of b/R_g, and the scattering is more significant as the value of b/R_g becomes smaller. This can be explained in part by thinking the conformation of DNA at impact. If the value of b/R_g is large, there is a high probability that both ends of the chain are located on the same side of the obstacle for a sufficiently long chain. This will lead to a very short lived W-collision since it will be unlikely for one end of the chain to unravel and extend around the other side of the obstacle. However, we did not observe a clear W-collision with our λ-DNA experiment. This is probably because λ-DNA is not long enough to hook around the post with W-configuration. When both ends of the chain are located on the same side of the post, λ-DNA rolls-off instead of hooking in most cases, as will be discussed in a later section. When the two ends of the chain are located on the opposite sides of the post for large values of b/R_g, it is likely that the collision leads to a fairly short-lived X-collison, and this is what we observed most frequently in our λ-DNA experiment; remember that, in an X-collision, the shorter arm starts retracting from the post before the longer arm is fully stretched. Thus, we should see a small scattering of data at large values of b/R_g, and this is consistent with our results.

If the value of b/R_g is small, it is more likely that two ends of the chain are located on opposite sides of the post, and the chain is likely to go through either a J- or U-collision. It is difficult to make a clear distinction between J- and U-collisions on the criteria of the hooking time. A large scattering of hooking times for J and U-collisions are also reported for 1.6 μm diameter PDMS post by Randall and Doyle [60].

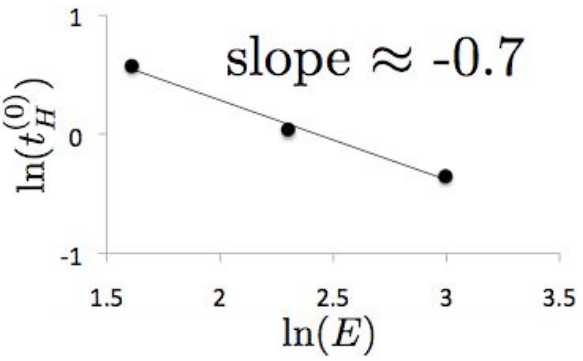

Figure 4.11: *A linear function fitted with the three intercept points at b/R_g= 0 to find the scaling on the electric field strength.*

In addition, the intercepts of the plots in Figure 4.10 correspond to the average hooking time at zero impact parameter ($\ln(t_{\mathrm{H}}^{(0)}) = 0.57$ for $E = 5$ V/cm, 0.03 for $E = 10$ V/cm, and -0.35 for $E = 20$ V/cm). From the plot of the intercepts, we can find the power law on the electric field strength (Figure 4.11). The plot shows the scaling of the electric field to be -0.7 . This is not in agreement with the prediction by Sevick and Williams as their prediction shows a scaling of -1. One of the reasons for this discrepancy comes from the difference between the simulation modeling and actual experiment. In the simulation, it is assumed that the molecule is in a strong stretching regime so that when hooked around the post, the length of the chain is approximately the same as the contour length of the molecule, L. However, as seen in Figure 4.8, the DNA molecules are not fully stretched even at $E = 20$ V/cm in our experiment; recall that the contour length of λ-DNA is ~ 21 μm.

To explain the $\mathrm{E}^{-0.7}$ power law dependence, we searched for a model that fits our experimental result. The experimental study by Randall and Doyle [60] shows that the hooking time by rope-over-pulley model can be estimated by replacing the length of the chain, L, with an incomplete extension of the chain, $\mathcal{L} = \phi L$, and the average hooking time should scale like

$$\langle t_H^{(0)} \rangle \approx \frac{\mathcal{L}}{\mu E} = \frac{\phi L}{\mu E}. \tag{4.2}$$

Assuming that the friction on the chain during hooking is proportional to the length of the stretched chain, we can write the friction force as

$$F = \mu E \eta \mathcal{L} = \mu E \eta \phi L. \tag{4.3}$$

The worm-like chain (WLC) model describes the tension force during hooking in a high stretching regime as [62],

$$\frac{F l_k}{k_B T} = \frac{1}{2(1-\phi)^2}. \tag{4.4}$$

Substituting Eq 4.3 into this WLC equation, we get

$$\frac{\mu E \eta \phi L l_k}{k_B T} = \frac{1}{2(1-\phi)^2}. \tag{4.5}$$

If we define the Péclet number as

$$\mathrm{Pe} = \frac{\mu E \eta L l_k}{k_B T}, \tag{4.6}$$

then, we can rewrite the WLC equation as

$$\mathrm{Pe}\phi = \frac{1}{2(1-\phi)^2}. \tag{4.7}$$

Rearranging the equation leads to

$$\phi^3 - 2\phi^2 + \phi - (2\mathrm{Pe})^{-1} = 0. \tag{4.8}$$

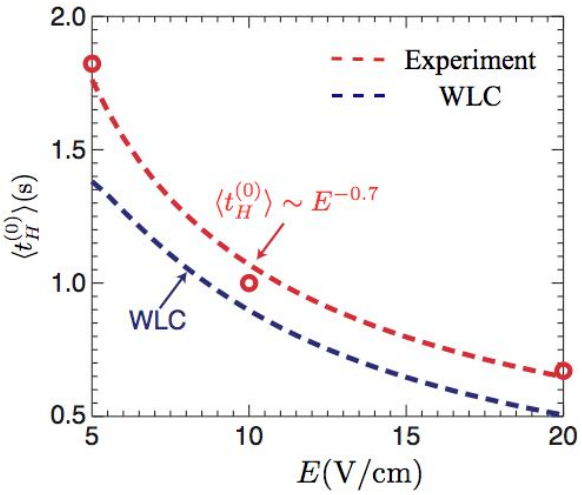

Figure 4.12: *Comparison of the prediction by WLC model and the experimental result.*

We solved this equation for an interval of $5 \leq \mathrm{E} \leq 20$ and the solutions were plugged into Eq 4.2 to find the hooking time. Figure 4.12 compares the prediction by the WLC model and our experimental result. It shows that the WLC model matches well with our experimental result in terms of the functional form and order of magnitude accuracy.

4.6 Hooking probability

When the value of b/R_g is large, there is a large probability that the DNA does not hook around the post and instead rolls off around the post. Such a collision is generally called a roll-off collision. Saville and Sevick [38] showed in their computational study that the roll-off collision leads to a size-independent collision time and cannot be used for size separation. In this section, we discuss our measurement of collision probability as a function of b/R_g.

Randall and Doyle [63] simulated the collision probability as a function of b/R_g using an obstacle with $R_{obs} = 0.8$ μm and studied how the hooking probability changes as the Deborah number is changed. The Deborah number, De, is the ratio of the rate of maximum DNA deformation to DNA relaxation in an obstacle induced electric field gradient, and it is expressed as $De = 2\mu E\tau/R_{obs}$, where μ is the electrophoretic mobility and τ is the relaxation time [63]. Their simulation shows that the hooking probability becomes ≈ 0 at the b/R_g value of around 1.5 and that the hooking probability increases as De is increased as shown in Figure 4.13. Their simulation study also shows that, for a point size obstacle, the hooking probability curve has a general flipped S-shape with a saturation value of $b/R_g \approx 0.4$ (point limit).

In our study, we changed the electric field strengths between 5, 10, and 20 V/cm and calculated De assuming that μ =1.7 x 10^{-4} cm^2/Vs and τ = 0.19 sec [63]. For measurement purposes, we define a roll-off collision as one in which the molecule does not occupy the four quadrants of the obstacle coordinate system. Figure 4.14 shows a typical roll-off collision observed in our system. The molecule goes through only a small deformation during the collision and advects around one side of the nanowire. Remember that the nanowires are tilted in random directions, and this makes an accurate measurement of b somewhat difficult. We measured the impact point of a nanowire by carefully looking at the image at impact. Collecting the impact parameters for all hooking and roll-off events, we calculated the hooking probability.

Figure 4.15 shows the plots of the hooking probability for $E = 5$, 10, and 20 V/cm. It is seen that the hooking probability at small b/R_g values is highest for $E = 20$ V/cm among three field strengths and smallest for $E = 5$ V/cm. This can be explained in terms of the contribution from random diffusive motion. For a high electric field, the motion of the molecule is dominated by the electro-hydrodynamic force and the diffusion is negligible. In other

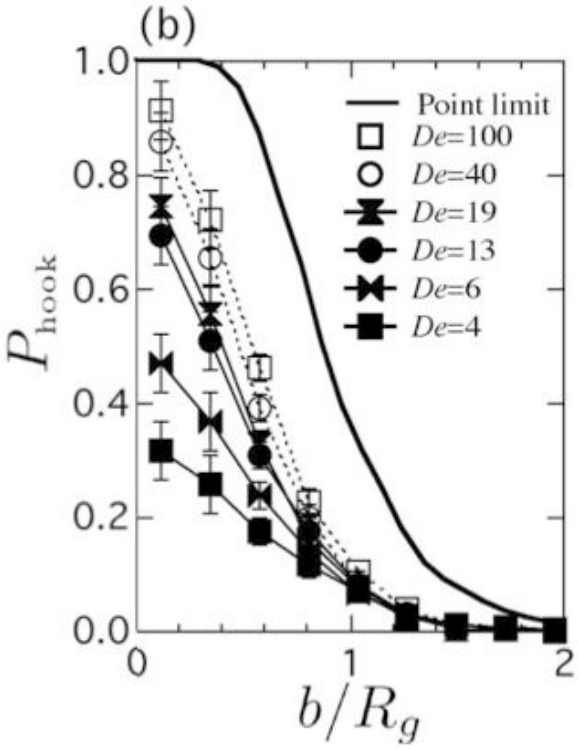

Figure 4.13: *Hooking probability prediction with an obstacle of* R_{obs}*= 0.8 μm. Reprinted from Randall and Doyle [63]*

Figure 4.14: *Example of roll-off collision. The red dots show the location of nanowire. The scale bar is 5 μm.*

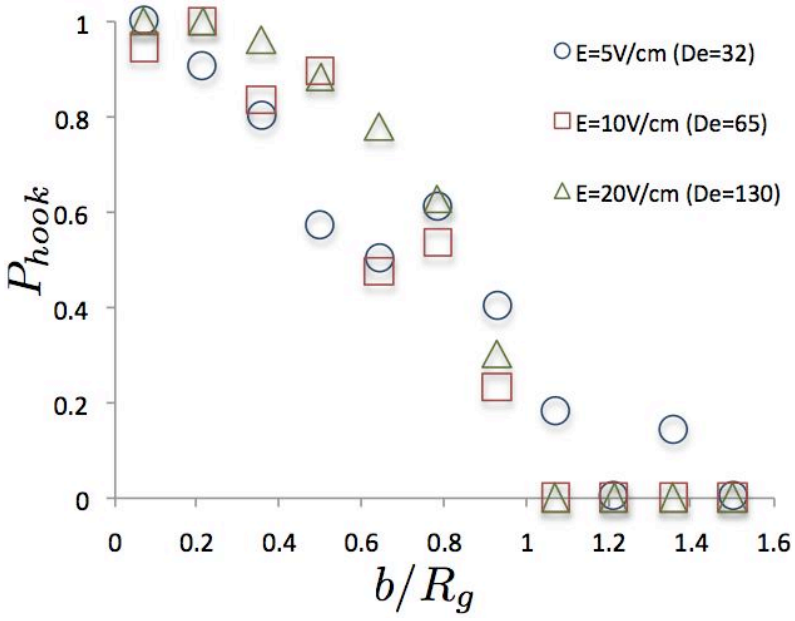

Figure 4.15: *Plot of hooking probability v.s.* b/R_g *for the electric field strengths of 5 V/cm, 10V/cm, and 20 V/cm. Each bin has a width of 0.14*

words, the motion by the electric field is faster than DNA can reorient itself by diffusive motion, *i.e.* $\mu E \gg R_g/\tau$ where τ is the chain's relaxation time (the time it takes to diffuse over its own size) [64]. Thus, the hooking probability is purely geometric, and the molecule should always hook around the post for a sufficiently small value of b/R_g. However, in the case of a weak electric field, random diffusive motion could have a significant contribution during impact and unraveling; DNA could reorient itself to escape from the post without hooking by its random diffusion before the molecule extends around the nanowire by the electric force [65] . Thus, the hooking probability at weak electric field is smaller than high electric field for small values of b/R_g.

For large values of b/R_g, the hooking probability at weak electric field could be higher than the strong electric field. With a similar argument, the large contribution from random diffusion makes possible for the chain to reorient itself during collision to hook around the post, thus increasing the probability

of hooking. In contrast, at high electric field, the DNA motion is dominated by electric field so that the molecule is more likely to simply roll-off around the post for a large value of b/R_g.

It is also worth comparing our hooking probability measurements with the simulation by Randall and Doyle in terms of the Deborah number. The obstacle employed in their simulation is a 1.6 μm diameter insulating post, which is slightly larger than the size of λ-DNA. Recall that the electric field lines deflect around an insulating obstacle. As the molecule comes closer to an insulating post, it feels a force that stretches the molecule around the post before collision. The effect of the electric field line gradients becomes larger as the size of the obstacle increases. Randall and Doyle [63] showed in their study that the hooking probability increases as De is increased. They attribute this increase of hooking probability to the enhanced effect of the obstacle-induced electric field gradients. Their study shows that the hooking probability saturates below the point size limit as De is increased above $\sim$ 40. Comparing their results with our experimental results, we can see that the hooking probability for our experiment is higher than their simulation for the similar value of De. This can be explained partly by considering the size of the ZnO nanowires used for our experiment. Recall that the size of the nanowire is 200-300 nm diameter, almost one order of magnitude smaller than the size of λ-DNA. Therefore, even when the DNA molecule comes in close proximity of the nanowire, the DNA will feel little effect of electric field gradients that might otherwise deflect the molecule away from the obstacle as in the case of large obstacle. This accounts for the higher hooking probability observed in our experiment than in the simulation for the similar value of De.

4.7 Conclusion

In this thesis research, we fabricated ZnO nanopillar array inside a microfluidic channel using a bottom-up approach without pre-nanopatterning for the first time and used it for the study of large DNA electrophoresis. Our developed chip has the potential to separate both small and large DNA fragments since the fabrication offers a facile method to control the nanopost density. It can be also used to conduct scientific studies of various types of DNA-nanopost interaction at an affordable cost; until now, only PDMS or silicon-based posts with much larger size or a dense nanopillar array was used for such purposes.

In our analytical study of the electrophoretic interaction of large DNA with the point size obstacle, we found that the hooking time is exponentially dependent on b/R_g, consistent with the theoretical prediction. We also found that the hooking probability for small values of b/R_g decreases as the electric field strength decreases.

For future work and practical application, we will need to conduct more studies to prove that DNA is not chemically and physically deteriorated by ZnO nanowires. It will be also beneficial to seek for a method to coat the ZnO nanowire surface to make it more stable in the buffer solution or to find an alternative buffer that is more compatible with ZnO.

Bibliography

[1] H. Hammond, L. Jin, Y. Zhong, C. Caskey, R. Chakraborty, Evaluation of 13 short tandem repeat loci for use in personal identification applications., American Journal of Human Genetics 55 (1) (1994) 175–189.

[2] V. Lyssenko, A. Jonsson, P. Almgren, N. Pulizzi, B. Isomaa, T. Tuomi, G. Berglund, D. Altshuler, P. Nilsson, L. Groop, Clinical risk factors, DNA variants, and the development of type 2 diabetes, The New England Journal of Medicine 359 (21) (2008) 2220–2232.

[3] H. Blauw, L. Franke, C. Saris, S. De Jong, V. De Jong, F. Baas, R. Van't Slot, H. Schelhaas, A. Birve, K. Sleegers, et al., Genetic variation in DPP6 is associated with susceptibility to amyotrophic lateral sclerosis, Nature Genetics 40 (1) (2008) 29–31.

[4] O. Bakajin, T. A. J. Duke, J. Tegenfeldt, C. F. Chou, S. S. Chan, R. H. Austin, E. C. Cox, Separation of 100-kilobase DNA molecules in 10 seconds, Analytical Chemistry 73 (24) (2001) 6053–6056.

[5] W. D. Volkmuth, T. Duke, M. C. Wu, R. H. Austin, A. Szabo, DNA electrodiffusion in a 2D array of posts, Physical Review Letters 72 (13) (1994) 2117–2120.

[6] L. R. Huang, J. O. Tegenfeldt, J. J. Kraeft, J. C. Sturm, R. H. Austin, E. C. Cox, A DNA prism for high-speed continuous fractionation of large

DNA molecules, Nature Biotechnology 20 (10) (2002) 1048–1051.

[7] P. S. Doyle, J. Bibette, A. Bancaud, J. L. Viovy, Self-assembled magnetic matrices for DNA separation chips, Science 295 (5563) (2002) 2237–2237.

[8] N. Kaji, Y. Tezuka, Y. Takamura, M. Ueda, T. Nishimoto, H. Nakanishi, Y. Horiike, Y. Baba, Separation of long DNA molecules by quartz nanopillar chips under a direct current electric field, Analytical Chemistry 76 (1) (2004) 15–22.

[9] Y. C. Chan, Y. Lee, Y. Zohar, High-throughput design and fabrication of an integrated microsystem with high aspect-ratio sub-micron pillar arrays for free-solution micro capillary electrophoresis, Journal of Micromechanics and Microengineering 16 (4) (2006) 699–707.

[10] R. Ogawa, H. Ogawa, A. Oki, S. Hashioka, Y. Horiike, Fabrication of nano-pillar chips by a plasma etching technique for fast DNA separation, Thin Solid Films 515 (12) (2007) 5167–5171.

[11] W. Russel, W. Russel, D. Saville, W. Schowalter, Colloidal Dispersions, Cambridge University Press, 1992.

[12] J. L. Viovy, Electrophoresis of DNA and other polyelectrolytes: Physical mechanisms, Reviews of Modern Physics 72 (3) (2000) 813–872.

[13] G. S. Manning, Limiting laws and counterion condensation in polyelectrolyte solutions I. Colligative properties, The Journal of Chemical Physics 51 (1969) 924–933.

[14] P. Hiemenz, T. Lodge, Polymer Chemistry 2nd Edition, CRC Press, 2007.

[15] N. C. Stellwagen, C. Gelfi, P. G. Righetti, The free solution mobility of DNA, Biopolymers 42 (6) (1997) 687–703.

[16] L. S. Lerman, H. L. Frisch, Why does the electrophoretic mobility of DNA in gels vary with the length of the molecule?, Biopolymers 21 (5) (1982) 995–997.

[17] O. J. Lumpkin, B. H. Zimm, Mobility of DNA in gel electrophoresis, Biopolymers 21 (11) (1982) 2315–2316.

[18] C. Heller, T. Duke, J. L. Viovy, Electrophoretic mobility of DNA in gels. II: Systematic experimental study in agarose gels, Biopolymers 34 (2) (1994) 249–259.

[19] T. A. J. Duke, A. N. Semenov, J. L. Viovy, Mobility of a reptating polymer, Physical Review Letters 69 (22) (1992) 3260–3263.

[20] D. C. Schwartz, C. R. Cantor, Separation of yeast chromosome-sized DNAs by pulsed field gradient gel electrophoresis., Cell 37 (1) (1984) 67–75.

[21] C. Turmel, E. Brassard, G. W. Slater, J. Noolandi, Molecular detrapping and band narrowing with high frequency modulation of pulsed field electrophoresis, Nucleic Acids Research 18 (3) (1990) 569–575.

[22] J. Sudor, M. V. Novotny, Separation of large DNA fragments by capillary electrophoresis under pulsed-field conditions, Analytical Chemistry 66 (15) (1994) 2446–2450.

[23] Y. Kim, M. D. Morris, Ultrafast high resolution separation of large DNA fragments by pulsed-field capillary electrophoresis, Electrophoresis 17 (1) (1996) 152–160.

[24] T. Duke, R. Austin, E. Cox, S. Chan, Pulsed-field electrophoresis in microlithographic arrays, Electrophoresis 17 (6) (1996) 1075–1079.

[25] J. Han, H. G. Craighead, Separation of long DNA molecules in a microfabricated entropic trap array, Science 288 (5468) (2000) 1026–1029.

[26] J. Han, S. W. Turner, H. G. Craighead, Entropic trapping and escape of Long DNA molecules at submicron size constriction, Physical Review Letters 83 (8) (1999) 1688–1691.

[27] S. W. P. Turner, M. Cabodi, H. G. Craighead, Confinement-induced entropic recoil of single DNA molecules in a nanofluidic structure, Physical Review Letters 88 (12) (2002) 128103.

[28] M. Cabodi, S. Turner, H. Craighead, Entropic recoil separation of long DNA molecules, Analytical Chemistry 74 (20) (2002) 5169–5174.

[29] T. A. J. Duke, R. H. Austin, Microfabricated sieve for the continuous sorting of macromolecules, Physical Review Letters 80 (7) (1998) 1552–1555.

[30] D. Ertaş, Lateral separation of macromolecules and polyelectrolytes in microlithographic arrays, Physical Review Letters 80 (7) (1998) 1548–1551.

[31] R. H. Austin, Continuous separation of biomolecules by the laterally asymmetric diffusion array with out-of-plane sample injection, Electrophoresis 23 (20) (2002) 3496–3503.

[32] C. F. Chou, O. Bakajin, S. W. P. Turner, T. A. J. Duke, S. S. Chan, E. C. Cox, H. G. Craighead, R. H. Austin, Sorting by diffusion: An asymmetric obstacle course for continuous molecular separation, Proceedings of the National Academy of Sciences 96 (24) (1999) 13762–13765.

[33] W. D. Volkmuth, R. H. Austin, DNA electrophoresis in microlithographic arrays, Nature 358 (6387) (1992) 600–602.

[34] E. M. Sevick, D. R. M. Williams, Motion of a polyelectrolyte chain hooked around a post, Physical Review E 50 (5) (1994) 3357–3360.

[35] G. I. Nixon, G. W. Slater, DNA electrophoretic collisions with single obstacles, Physical Review E 50 (6) (1994) 5033–5038.

[36] E. M. Sevick, D. R. M. Williams, Collision of a field-driven polymer with a post: Electrophoresis in microlithographic arrays, Physical Review Letters 76 (14) (1996) 2595–2598.

[37] P. André, D. Long, A. Ajdari, Polyelectrolyte/post collisions during electrophoresis: Influence of hydrodynamic interactions, The European Physical Journal B-Condensed Matter 4 (3) (1998) 307–312.

[38] P. M. Saville, E. M. Sevick, Collision of a field-driven polymer with a finite-sized obstacle: A Brownian dynamics simulation, Macromolecules 32 (3) (1999) 892–899.

[39] P. D. Patel, E. S. G. Shaqfeh, A computational study of DNA separations in sparse disordered and periodic arrays of posts, The Journal of Chemical Physics 118 (6) (2003) 2941–2951.

[40] P. S. Doyle, B. Ladoux, J. L. Viovy, Dynamics of a tethered polymer in shear flow, Physical Review Letters 84 (20) (2000) 4769–4772.

[41] C. Goubault, J. L. Viovy, Quantitative microfluidic separation of DNA in self-assembled magnetic matrixes, Analytical Chemistry 76 (13) (2004) 3770–3776.

[42] G. C. Randall, P. S. Doyle, Collision of a DNA polymer with a small obstacle, Macromolecules 39 (22) (2006) 7734–7745.

[43] G. M. Whitesides, E. Ostuni, S. Takayama, X. Jiang, D. E. Ingber, Soft lithography in biology and biochemistry, Annual Reviews in Biomedical Engineering 3 (1) (2001) 335–373.

[44] K. Inatomi, S. Izuo, S. Lee, H. Ohji, S. Shiono, Electrophoresis of DNA in micro-pillars fabricated in polydimethylsiloxane, Microelectronic Engineering 70 (1) (2003) 13–18.

[45] J. Ou, J. Cho, D. W. Olson, K. D. Dorfman, DNA electrophoresis in a sparse ordered post array, Physical Review E 79 (6) (2009) 61904.

[46] Y. Xia, G. M. Whitesides, Soft lithography, Annual Reviews in Materials Science 28 (1) (1998) 153–184.

[47] Y. Chen, E. Roy, Y. Kanamori, M. Belotti, D. Decanini, Soft nanoimprint lithography, Proceedings of SPIE 5645 (2005) 283–288.

[48] J. Shi, A. P. Fang, L. Malaquin, A. Pépin, D. Decanini, J. L. Viovy, Y. Chen, Highly parallel mix-and-match fabrication of nanopillar arrays integrated in microfluidic channels for long DNA molecule separation, Applied Physics Letters 91 (2007) 153114.

[49] C. Kuo, K. Wei, C. Lin, J. Shiu, P. Chen, Nanofluidic system for the studies of single DNA molecules, Electrophoresis 29 (14) (2008) 2931–2938.

[50] M. Wang, C. H. Ye, Y. Zhang, H. X. Wang, X. Y. Zeng, L. D. Zhang, Seed-layer controlled synthesis of well-aligned ZnO nanowire arrays via a low temperature aqueous solution method, Journal of Materials Science: Materials in Electronics 19 (3) (2008) 211–216.

[51] L. E. Greene, M. Law, D. Tan, M. Montano, J. Goldberger, G. Somorjai, P. Yang, General route to vertical ZnO nanowire arrays using textured ZnO seeds, Nano Letters 5 (7) (2005) 1231–1236.

[52] J. B. Baxter, A. M. Walker, K. van Ommering, E. S. Aydil, Synthesis and characterization of ZnO nanowires and their integration into dye-sensitized solar cells, Nanotechnology 17 (11) (2006) 304–312.

[53] D. Bartolo, G. Degré, P. Nghe, V. Studer, Microfluidic stickers, Lab on a Chip 8 (2) (2008) 274–279.

[54] C. Lin, G. Lee, B. Chang, G. Chang, A new fabrication process for ultra-thick microfluidic microstructures utilizing SU-8 photoresist, Journal of Micromechanics and Microengineering 12 (5) (2002) 590–597.

[55] G. Luurtsema, Spin coating for rectangular substrates, Ph.D. thesis, University of California (1997).

[56] E. Sevick, D. Williams, Collision of a field-driven polymer with a post: Electrophoresis in microlithographic arrays, Physical Review Letters 76 (14) (1996) 2595–2598.

[57] A. Degen, M. Kosec, Effect of pH and impurities on the surface charge of zinc oxide in aqueous solution, Journal of the European Ceramic Society 20 (6) (2000) 667–673.

[58] G. Parks, P. Bruyn, The zero point of charge of oxides, The Journal of Physical Chemistry 66 (6) (1962) 967–973.

[59] A. Larsson, C. Carlsson, M. Jonsson, B. Albinsson, Characterization of the binding of the fluorescent dyes YO and YOYO to DNA by polarized light spectroscopy, Journal of the American Chemical Society 116 (19) (1994) 8459–8465.

[60] G. Randall, P. Doyle, Collision of a DNA Polymer with a Small Obstacle, Macromolecules 39 (22) (2006) 7734–7745.

[61] G. Randall, P. Doyle, DNA deformation in electric fields: DNA driven past a cylindrical obstruction, Macromolecules 38 (6) (2005) 2410–2418.

[62] O. Bakajin, T. Duke, C. Chou, S. Chan, R. Austin, E. Cox, Electrohydrodynamic stretching of DNA in confined environments, Physical Review Letters 80 (12) (1998) 2737–2740.

[63] G. Randall, P. Doyle, Electrophoretic collision of a DNA molecule with an insulating post, Physical Review Letters 93 (5) (2004) 58102.

[64] P. André, D. Long, A. Ajdari, Polyelectrolyte/post collisions during electrophoresis: Influence of hydrodynamic interactions, The European Physical Journal B-Condensed Matter and Complex Systems 4 (3) (1998) 307–312.

[65] S. Holleran, R. Larson, Multiple regimes of collision of an electrophoretically translating polymer chain against a thin post, Macromolecules 41 (13) (2008) 5042–5054.